Mutual transformations of fractional-order and integer-order optical vortices

C. N. Alexeyev, Yu. A. Egorov, and A. V. Volyar
V. I. Vernadsky Crimean Federal University, Vernadsky Prospekt, 4, Simferopol, 295007, Ukraine
(Received 27 June 2017; published 5 December 2017)

In this paper we studied the shaping and evolution of singular beams bearing optical vortices with fractional topological charges both in uniform and nonuniform anisotropic media. Starting from representation of the fractional-order vortex states as a superposition of an infinite number of integer-order vortices with certain energy distributions (the vortex spectra) we showed that the smooth wave front of the fractional vortex beam can either decay into an asymmetric array of integer-order vortices or, vice versa, the array of optical vortices can form a smooth helicoid-shaped wave front. We showed that by superimposing a finite number of the fractional-order vortex beams one can shape symmetric singular beams with arbitrary valued topological charges. We demonstrated that in biaxial crystals under the condition of the conical diffraction the fractional-order vortices are unstable. We also demonstrated that the circular fiber array with a space-variant birefringence is an appropriate medium for fractional-order vortex beams. In such arrays the supermodes may bear the half-integer-order vortices in circular components. Forming such supermodes plays a decisive role in evanescent-coupling assisted phase locking of individual fiber modes combined with tunneling of polarization states between anisotropic fibers in the array. We showed that the integer-charge phase increment in a fractional-order supermode consists of two half-integer-charge phase contributions. The explicit phase contribution is connected with the Pancharatnam-Berry phase that arises due to the phenomenon of nonadiabatic following. The implicit half-integer-charge phase contribution (or the "hidden phase") happens due to the sign alteration of the amplitude factors in the field components that corresponds to the wave-front cuts. We have also made the comparison of the hidden and hydrodynamic phases in superfluidic fractional-charge vortices with analogous phases in fractional-order supermodes. We have established that in the optical case the hidden phase corresponds to the hydrodynamic phase in superfluids, whereas the hidden superfluidic phase is the analog of the optical Pancharatnam-Berry phase in supermodes.

DOI: 10.1103/PhysRevA.96.063807

I. INTRODUCTION

The past recent years of singular optics development [1] have been marked by a surge of interest in optical vortices with fractional topological charges [2–13]. The first announcement of the fractional-order vortex propagation instability in principle was reported by Soskin *et al.* [2,3] for the vortices produced by a computer-generated hologram. The authors observed experimentally the evolution of vortex beams with different half-integer-order topological charges. If the vortex beam at the hologram has a nearly C-shaped form, far from the hologram the beam breaks into a great number of integer-order vortices.

Later, starting from an analogy with the Aharonov-Bohm effect in quantum mechanics and hydrodynamics [4], Berry *et al.*, theoretically showed the splitting of an optical vortex of the fractional order into an infinite chain of integer-order vortices [5]. Berry and co-workers noted a deep analogy between the quantum and the optical singularities. In addition, they observed that fractional-order vortex propagation results inevitably in the decay of the initial phase structure in free space; i.e., the fractional-order vortex beams are structurally unstable under propagation. Fractional-order vortex states have been observed also in superfluid ^{3}He [6], in mesoscopic rings of superconductors [7], and in other condensed-matter systems, ranging from Bose-Einstein condensates to spin-triplet superconductors [8–10].

These reports stimulated a new chain of theoretical and experimental investigations [11–15] that confirmed the decay of fractional-order vortices into an infinite number of integer-order vortices. Although most of the mathematical models of the fractional vortices are based on the Bessel-Gaussian (BG) beam representation (see, e.g., [13,14]), the authors of Ref. [15] supplemented the analysis with Laguerre-Gaussian (LG) beams. The fact is that BG and LG beam representations make different contributions to vortex spectra of fractional vortex beams that should be taken into account for experimental implementations [16]. On the other hand, the authors of Ref. [17] found a peculiar behavior of the vortex beam with a half-order topological charge for the erf-Gaussian (erf−G) beams. The smooth wave front of the fractional vortex beam can either decay into an asymmetric array of integer-order vortices or, vice versa, the array of optical vortices can form a smooth wave front with a helicoid-shaped phase distribution. This is possible only if the Gouy phases of all integer-order vortex beams in the vortex array are matched with each other.

The authors of Ref. [18] also remarked on an unusual behavior of the specific orbital angular momentum (OAM) l_z. At first sight it seems that a topological charge value p follows the value of the specific OAM $l_z \approx p$. In some papers [14,19] the authors observed small oscillations of OAM near the line $l_z = p$. However, the computer simulation of the process and the physical analysis [18] revealed a complex behavior of the function $l_z(p)$. For larger values of p ($p > 10$) the amplitude starts to oscillate between minimum values $l_{z,\,\mathrm{min}} \approx 0$ and maximum values $l_z = p = m$, where the index m is the integer-order topological charge of the vortex. The presented results are the evidence of a complex interference coupling between a great number of integer-order vortices in a fractional-order vortex beam.

Another unexpected property of the fractional-order vortex beams was revealed in Ref. [20]. The authors experimentally answered the question: Can the fractional-order vortex beams

control the states of the integer-order ones? They got a positive answer using two beams: the pump and the probe beams. The pump beam is of a topological dipole field consisting of two half-order vortices with charges of opposite sign. The pump beam creates appropriate conditions in a nonlinear medium for propagation of the probe singular beam with a smaller intensity. Changing parameters of the dipole they could steer the state of the probe beam. In fact, the fractional-order topological dipole was not destroyed inside the nonlinear medium forming the waveguide channel for the probe beam.

However, the above example of the structural stability of the fractional-order beams in nonlinear media is not the only way to preserve a vortex structure of such complex fields. The authors of Ref. [21] considered the properties of the complex fields in a discrete birefringent fiber array and revealed that half-integer-order vortices are the supermodes of such a linear optical system; i.e., the fractional-order vortex beams could propagate without destroying their structure.

Thus the fractional-order vortex beams possess a fertile potential of useful properties that call for implementation. The prior problems that should be considered, from our point of view, can be outlined as follows: (1) studying the physical properties of the field propagating in free space that are responsible for decaying and recovery of the initial structure of the beam wave front inside the fractional-order vortex beams; (2) shaping the singular beams with preassigned properties on the base of a finite superposition of fractional-order vortex beams; (3) search for optical media where the fraction-order vortex beams are eigenmodes (i.e., structurally propagation-stable wave constructions); (4) development of the measurement technique and the study of vortex spectra of the singular beam scattered by different linear and nonlinear media. We will focus our attention only on the first three interrelated problems of the above items.

The aim of our paper is to consider the key features of the fractional-order vortex beams in free space and space-variant anisotropic media—namely, to study (i) the properties of the beams with half-integer-charge vortices; (ii) the shaping of integer-order beams and their stability under propagation as a superposition of fractional-order vortex beams; (iii) structural stability of the beams in biaxial crystals under the condition of the conical diffraction; (iiii) the properties of the beams in a circular fiber array with a space-variant birefringence.

The paper is organized as follows. In Sec. II we will treat the propagation of fractional-order vortices in free space and uniform media. Our special interest is optical beams with half-integer-order vortices. In addition, we will focus our attention on the mutual transformations of integer- and fractional-order vortex beams and their structural stability. Eigenstates of the conical diffraction process in the form of the fractional-order vortices are studied in Sec. III. The consideration in Sec. IV is accompanied by the analysis of the physical properties of supermodes bearing half-integer vortices. We concentrate attention on the following nonadiabatic effect responsible for shaping the supermodes with fractional-order vortices.

II. FRACTIONAL-ORDER VORTEX BEAMS IN FREE SPACE

As has been mentioned above, the choice of the basic representation of a fractional optical vortex in the form of BG or LG beam superposition plays a key part in shaping the spectral content of integer-order vortices in the complex field. From our point of view, the BG beams are appropriate units for our theoretical treatment because they enable us to present the obtained results in a compact form suitable for a computer simulation. Besides, such a representation complies with the techniques of experimental measurements of the vortex spectrum [12]. In the following subsections we set a task to uncover the basic properties of different types of fractional-order vortex beams and to build up from them the integer-order vortex beams on the basis of BG beams.

A. Fractional vortex states

Let us consider, at first, typical vector supermodes in free space or a uniform isotropic medium made up of the BG beams. We focus our attention on monochromatic wave beams with the carrier frequency ω that enables us to exploit the vector Helmholtz equation for the vector potential $\mathbf{A}$ under the condition of the Lorentz gauge [17]. The electric $\mathbf{E}$ and magnetic $\mathbf{H}$ fields can be defined as

$$\mathbf{E} = ik\left[\mathbf{A} + \frac{1}{k^2}\nabla(\nabla\cdot\mathbf{A})\right],\ \ \mathbf{H} = \nabla\times\mathbf{A}, \tag{1}$$

where k is the wave number.

Our interest is in the paraxial approximation where $|\partial_z^2\mathbf{A}| \ll |k^2\mathbf{A}|$ so that the longitudinal components E_z and H_z can be expressed in terms of the transverse $\mathbf{E}_\perp$ and $\mathbf{H}_\perp$ ones as

$$E_z \approx \frac{i}{k}\nabla_\perp\cdot\mathbf{E}_\perp,\ \ H_z \approx \frac{i}{k}\nabla_\perp\cdot\mathbf{H}_\perp,\quad \nabla_\perp \equiv \mathbf{e}_x\partial_x + \mathbf{e}_y\partial_y. \tag{2}$$

For the beam propagating along the z axis the complex amplitude $\tilde{\mathbf{A}}$ of the vector potential $\mathbf{A} = \tilde{\mathbf{A}}(x,y,z)\,e^{ikz}$ obeys the paraxial wave equation,

$$(\nabla_\perp^2 + 2ik\partial_z)\tilde{\mathbf{A}}_\perp = 0. \tag{3}$$

The choice of the vector $\mathbf{A}$ is defined by the type of the wave beam. If we take, for example, the vector $\mathbf{A}$ to be directed along the x axis (a linearly polarized basis), $\mathbf{A} = \mathbf{e}_x\tilde{A}_\perp\exp(ikz)$, then the solution to the vector wave equation is reduced to the scalar Eq. (3) for the function $\Psi(x,y,z) = \tilde{A}_\perp$ with the solution [22]

$$\Psi = NF(X,Y)\,G(x,y,z), \tag{4}$$

where

$$G(x,y,z) = \exp\left(i\frac{kr^2}{2Z}\right)\Big/ Z \tag{5}$$

stands for the Gaussian envelope, $Z = z - iz_0$, $z_0 = kw_0^2/2$ is the Rayleigh length with the radius of the beam waist w_0, $X = x/Z$, $Y = y/Z$, $N = w_0\exp(-\frac{K^2}{2ikZ})$, $r^2 = x^2 + y^2$, and K is the arbitrary beam parameter that can take on both the real and complex values.

At the same time the function $F(X,Y)$ obeys the two-dimensional Helmholtz equation,

$$\left(\frac{\partial^2}{\partial X^2} + \frac{\partial^2}{\partial Y^2} + K^2\right)F = 0. \tag{6}$$

In the cylindrical coordinates the solution to Eq. (6) can be written as

$$F_p(R,\varphi) = \int_0^{2\pi} \exp\{i[p\varphi' - KR\cos(\varphi' - \varphi)]\}d\varphi', \quad (7)$$

Here the parameter $p \in (-\infty,\infty)$ is real valued, $R^2 = X^2 + Y^2$. The real part of the parameter K is connected with the half angle θ of the plane wave's cone of the Bessel beam as $\mathrm{Re}(K) = \tan\theta = k_\perp/k_z \approx k_\perp/k$, where $k_\perp$ and k_z are the transverse and longitudinal components of the wave vector $\mathbf{k}$.

Such a representation of the beam charge p enables us to expand any regular complex beam into the series over different fractional-charged optical vortices just as it can be represented as decomposition over integer-order-charged ones.

To obtain the explicit form of the function F_p in Eq. (7) let us use the Fourier transformation,

$$e^{ip\phi} = \frac{e^{i\pi p}\sin(\pi p)}{\pi}\sum_{m=-\infty}^{\infty}\frac{e^{im\phi}}{p-m}. \quad (8)$$

The parameter p here can be regarded as a fractional topological charge, which is responsible for the set of integer-order vortices with topological charges $m = -\infty\cdots -1,0,1\cdots +\infty$ and the spectral vortex density $\rho(p) = (p-m)^{-1}$. When $p = m$ all the terms of the series vanish except for the term $e^{im\phi}$. In a general case the function $\rho(p)$ can be defined by a preassigned way as, for example, in Ref. [15] for LG beams, but for our purposes we restrict its dependence to $\rho(p) = (p-m)^{-1}$.

On the other hand, the definition of the Bessel function is

$$2\pi i^m J_m(KR) = \int_0^{2\pi}\exp\{i[m\phi + K\cos\phi]\}d\phi. \quad (9)$$

As a result, we find

$$|p\rangle = \Psi(r,\varphi,z,p) = 2NG(r,z)\sin(\pi p)e^{i\pi p} \times \sum_{m=-\infty}^{\infty}\frac{i^m e^{im\varphi}}{p-m}J_m(KR). \quad (10)$$

Thus the fractional topological charge p can serve as a global parameter of the complex optical beam. The obtained equation implies two possible propagation processes depending on the value of the K parameter. The real K parameter is associated with the phase front wreathed by a net of integer-charged vortices at the initial $z = 0$ plane. For example, when propagating, the vortices with $p = 1/2$ begin to form a group in such a way that the vortex net vanishes. There appears a smooth wave front looking like a helix with a phase shift $\Delta\Phi = \pi$ and a C-shaped intensity distribution. For the imaginary value of the K parameter, the process evolves in the opposite direction [17] (see also Fig. 1). Let us consider such a process in detail.

B. Asymmetric TE and TM mode beams

The fractional-order vortex beams permit us to construct unusual wave structures with broken axial symmetry. In contrast to the usual axially symmetric TE and TM modes with a local linear polarization in each point of the beam, the broken structure of the paraxial TE and TM mode beams with fractional-order $p = \pm 1/2$ vortices in each polarized component contains local elliptic polarizations. The broken symmetry of the vector field dictates the choice of the basis in the form of circularly polarized components.

From Eq. (2) we obtain for the TE mode ($E_z = 0,\ A_z = 0$)

$$\partial_x E_x = -\partial_y E_y \ \text{ or } \ \partial_x A_x = -\partial_y A_y, \quad (11)$$

and

$$\partial_x H_x = -\partial_y H_y \ \text{ or } \ \partial_x A_y = -\partial_y A_x, \quad (12)$$

for the TM mode ($H_z = 0,\ A_z = 0$).

It is convenient to employ the circularly polarized basis

$$A_+ = A_x - iA_y, \quad A_- = A_x + iA_y \quad (13)$$

and use complex coordinates,

$$u = x + iy = re^{-i\varphi}, \quad v = x - iy = re^{i\varphi}, \quad (14)$$

so that

$$\partial_u = \partial_x - i\partial_y = \frac{e^{-i\varphi}}{2}\left(\partial_r - \frac{i}{r}\partial_\varphi\right),$$
$$\partial_v = \partial_x + i\partial_y = \frac{e^{i\varphi}}{2}\left(\partial_r + \frac{i}{r}\partial_\varphi\right). \quad (15)$$

Then we find for the TE modes $A_+ = \partial_u\Psi_p$, $A_- = -\partial_v\Psi_p$ or

$$E_+ = N\left[\partial_u F_p + ik\frac{v}{2Z}F_p\right]G,$$
$$E_- = -N\left[\partial_v F_p + ik\frac{u}{2Z}F_p\right]G, \quad (16)$$

where the function F_p obeys Eq. (7).

In the paraxial cases, where $|\partial_{u,v}F_p| \ll k|F_p|$, we can use the approximation

$$E_+ \approx iNk\frac{v}{2Z}F_pG, \quad E_+ \approx -iNk\frac{u}{2Z}F_pG. \quad (17)$$

Similarly, we obtain the TM mode beams,

$$E_+ \approx iNk\frac{v}{2Z}F_pG, \quad E_+ \approx iNk\frac{u}{2Z}F_pG. \quad (18)$$

Half-order $(2n+1)/2$ vortex beams hold a special place among the variety of fractional-charged optical fields because they can be easily and reliably generated at the initial plane by q plates [23], photonic crystals [24], and arrays of microchip lasers [25]. Special types of singular beams with fractional topological charges and fractional OAM in the closed form (e.g., erf-G beams and others) have been recently considered in a number of papers [16,17,18,26]. In this subsection we will obtain the general closed form of the half-order vortex beams.

As a starting point we take Eq. (7) and rewrite it in the form

$$F_p(R,\varphi) = Ke^{i\frac{2n+1}{2}\varphi}\int_{-\varphi/2}^{\pi-\varphi/2}e^{i(2n+1)\phi}e^{-iKRos2\phi}d\phi. \quad (19)$$

In the following we will use the relations

$$\cos(2n+1)\phi d\phi = \sum_{j=0}^{[n+1/2]}(-1)^j C_n^{2j}\sin^{2j}\phi\cos^{n-2j}\phi d\phi$$

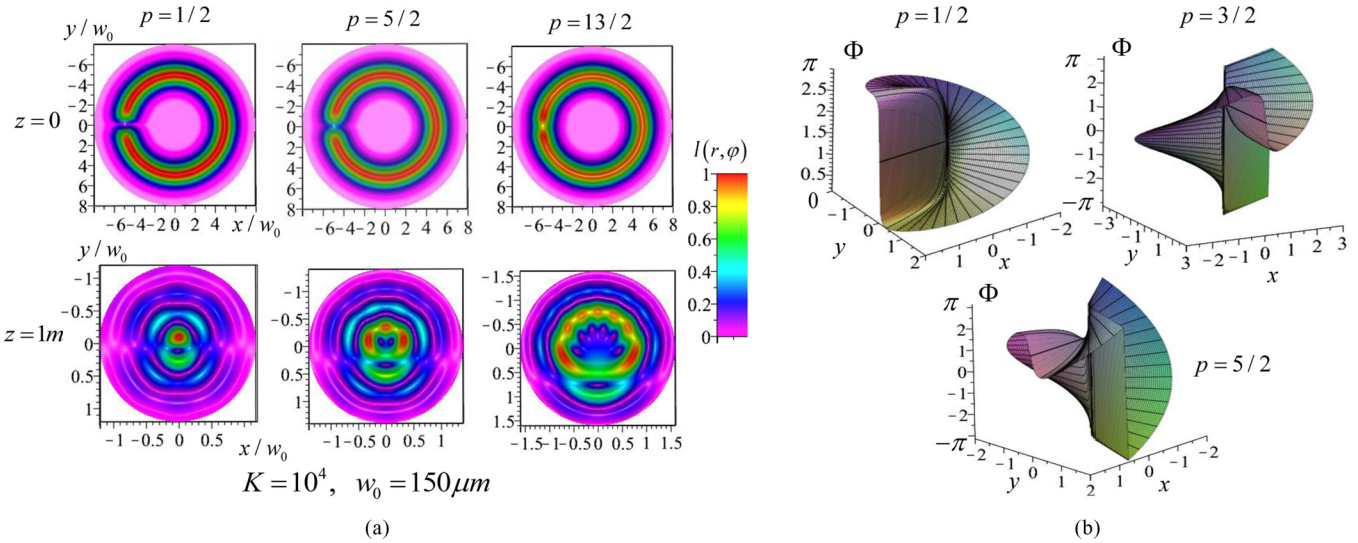

FIG. 1. (a) Intensity distributions $I(r,\varphi)$ of the of the E_+ components of Gamma-Gaussian (Γ-G) beams with different topological charges p at the initial plane $z = 0$ and at the far diffraction zone $z = 1$ m and (b) their phase distributions $\Phi(r,\varphi)$ at the initial plane $z = 0$.

$$= \sum_{j=0}^{[n+1/2]} \sum_{m=0}^{n-j} (-1)^{n-j} C_{2n+1}^{2j} C_{n-j}^{m} \times \sin^{2(j+m)}\phi \, d(\sin\phi),$$

$$\sin(2n+1)\phi d\phi = \sum_{j=0}^{n} (-1)^{j} C_{2n+1}^{j} \sin^{2j+1}\phi \cos^{2(n-j)}\phi d\phi$$

$$= -\sum_{j=0}^{n} \sum_{m=0}^{2j} (-1)^{m+j} C_{2n+1}^{j} C_{2j}^{m} \times \cos^{2(n-j+m)}\phi d(\cos\phi), \quad (20)$$

where C_n^m is the binomial coefficient, which, in particular, gives

$$\cos 3\phi d\phi = (1 - 4\sin^2\phi) d(\sin\phi),$$
$$\sin 3\phi d\phi = -(4\cos^2\phi - 1) d(\cos\phi). \quad (21)$$

Upon substitution of Eq. (20) into Eq. (19) and integration [27] we obtain

$$F_p = F_n = K e^{i\frac{2n+1}{2}\varphi} \left\{ \sum_{j=0}^{[n+1/2]} \sum_{m=0}^{n-j} (-1)^{n+j} C_{2n+1}^{2j} C_{n-j}^{m} F_{m,j}^{(s)} + \sum_{j=0}^{n} \sum_{m=0}^{2j} (-1)^{m+j} C_{2n+1}^{j} C_{2j}^{m} F_{m,j}^{(c)} \right\}, \quad (22)$$

where

$$F_{j,m}^{(s)} = \frac{\Gamma\left(j+m+\frac{1}{2}\right) - \Gamma\left(j+m+\frac{1}{2}, -2iKR\sin^2\frac{\varphi}{2}\right)}{(-2iKR)^{1/2+j+m}},$$
$$F_{j,m}^{(c)} = -\frac{\Gamma\left(j+m+\frac{1}{2}\right) - \Gamma\left(j+m+\frac{1}{2}, 2iKR\cos^2\frac{\varphi}{2}\right)}{(2iKR)^{1/2+j+m}}. \quad (23)$$

$\Gamma(n,x)$ stands for the incomplete Gamma function.

For example, the fractional beam with $p = 3/2$ is described by the expression

$$\Psi_{3/2} = \frac{NG}{\sigma} K \left\{ F_{3/2}^{(s)} + i F_{3/2}^{(c)} \right\} e^{i\frac{3}{2}\varphi},$$
$$F_{3/2}^{(s)} = -\left\{ 4\sqrt{\overline{R}} \sin\frac{\varphi}{2} e^{-\mathrm{Re}\sin^2\frac{\varphi}{2}} + \sqrt{\pi}(\overline{R} - 2) \times \mathrm{erf}\left(\sqrt{\overline{R}}\sin\frac{\varphi}{2}\right) \right\} \Big/ \sqrt{\overline{R}},$$
$$F_{3/2}^{(c)} = \left\{ 4\sqrt{-\overline{R}} \cos\frac{\varphi}{2} e^{-\mathrm{Re}\cos^2\frac{\varphi}{2}} - \sqrt{\pi}(\overline{R} + 2) \times \mathrm{erf}\left(\sqrt{-\overline{R}}\cos\frac{\varphi}{2}\right) \right\} \Big/ \sqrt{-\overline{R}},$$
$$\overline{R} = 2iKR. \quad (24)$$

It is useful to note that the function $\Psi_{3/2}$ in Eq. (24) is a periodic one with the period 2π despite the factors $\cos\frac{\varphi}{2}$ and $\sin\frac{\varphi}{2}$ in the function $F_{3/2}^{(c,s)}$. In order to prove it, it is necessary to take into account the factor $e^{i\frac{3}{2}\varphi}$ in the definition of the function $\Psi_{3/2}$ and the oddness of the function $\mathrm{erf}(x)$.

The above presented results form a family of asymmetric scalar vortex beams with $p = \pm(2n+1)/2$—the Gamma-Gaussian (Γ-G) beams. The Γ-G beams are the natural generalization of the erf−G beams [17] over all the set of half- integer-order vortex beams.

Typical representatives of the Γ-G family of singular beams are shown in Fig. 1. Thus the field distributions $I(r,\varphi)$ at the beam cross section depend essentially on the value of the K parameter. When the K parameter has a pure real value (see Fig. 1) the intensity distribution has a C-like profile at $z = 0$ with only half-integer-order vortices near the center (see, e.g., [17]). However, when propagating the intensity profile is drastically transformed, turning at $z \gg z_0$ into a broken Bessel beam with integer-order vortices scattering over the beam cross section. For the pure imaginary K parameter ($|K|$ is constant), the process is reversed.

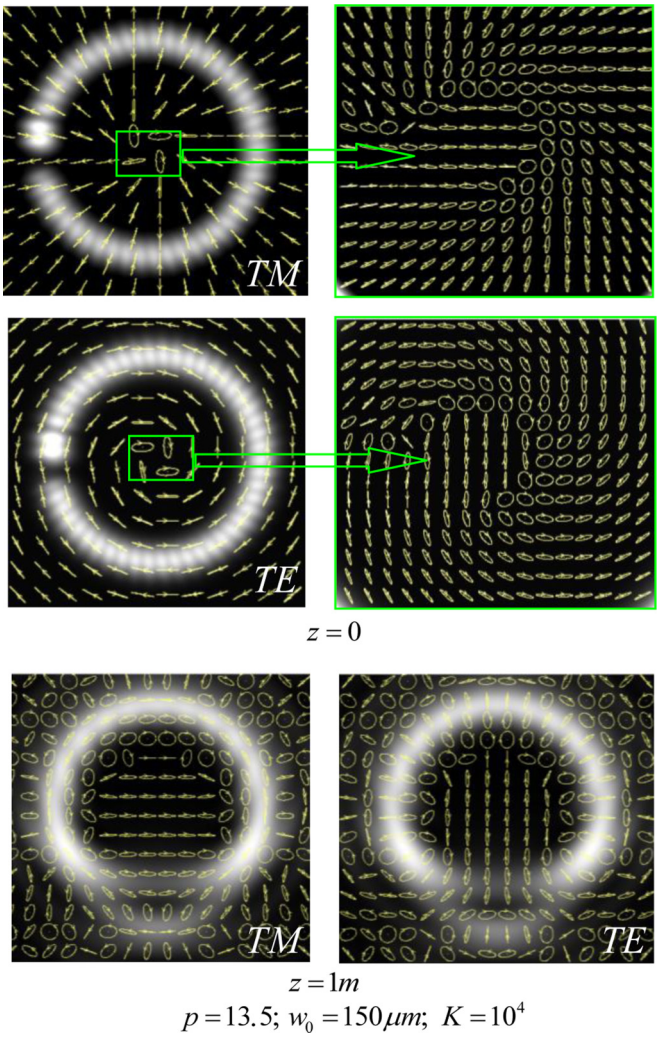

FIG. 2. The field distributions of the vector Γ-G beams for different topological charges on the background of the intensity distributions of the E_+ components. Callouts in the first two patterns illustrate a fine structure of the field polarization in a small center area.

The phase distributions shown in Fig. 1(b) illustrate complex phase structures for different half-order vortex beams. A smooth growth of the phase up to $\Phi = \pi/2$ for $p = 1/2$ is replaced by the phase oscillations in the broken second branch of the two-sheeted helicoid for the topological charge $p = 3/2$. The phase loss is $\Delta\Phi = \pi/2$. The same phase construction is observed for the topological charge $p = 5/2$ where the third branch of the three-sheeted helicoid also lacks the phase $\Delta\Phi = \pi/2$. All phase losses are accompanied by smooth variations. The sign alternation $p \to -p$ changes the direction of the helicoid twist.

All the above equations enable us to build a great number of asymmetric TE and TM beams. Some of them are shown in Fig. 2. The fine structure of these fields changes along the beam length, so that the beams are structurally unstable under propagation in free space. In contrast to standard TE and TM modes the asymmetric paraxial beam fields in Fig. 2 are elliptically polarized at each point with distinctive orientations of the ellipse axes. Near the optical axis the field tends to form

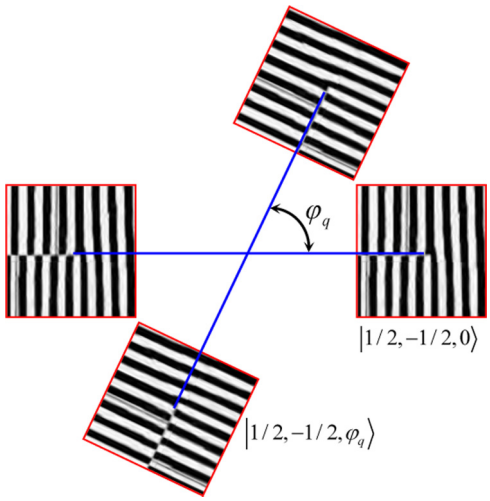

FIG. 3. The sketch of the topological dipole and its angular rotation. Interference patterns are associated with fractional vortices while the "fork" directions (upward or downward) set signs (plus or minus) of vortex topological charges.

two polarization singularities (the star or the lemon [12]). Far from the center the directions of the linear polarization are wound into Archimedean (for TE mode) and logarithmic (for TM mode) spirals.

The peculiar feature of the Γ-G beams is also their ability to assemble integer-order vortices into the fractional vortex at the far diffraction zone when the K parameter is real. The imaginary K parameter induces the reverse process—the fractional vortex decays into an infinite number of integer-order vortices. Such beam behavior reflects the inherent processes in the fractional-order vortex structures in contrast to vortex decaying. In essence, all the types of the above-considered fractional-order beams are structurally unstable under propagation.

C. Shaping the integer-order vortex beams

The key question of this subsection is the following. Can a superposition of the fractional-order vortex beams form a singular structure with a stable centered integer-order vortex?

First, we will analyze a dipole structure consisting of two orthogonal states $|p\rangle$ and $|-p\rangle$:

$$|p,-p\rangle = |p\rangle + |-p\rangle = Q\sum_{m=-\infty}^{\infty}\frac{i^m m e^{im\varphi}}{p^2-m^2}J_m(KR), \quad (25)$$

where $Q = 2NG(r,z)\sin(\pi p)e^{i\pi p}$. We can regard the state in Eq. (25) as the initial topological dipole.

After rotating the initial dipole through an angle $\varphi_q = \frac{\pi}{q}$ (see Fig. 3) so that $\varphi \to \varphi + \frac{\pi}{q}$ we obtain

$$|p,-p,q\rangle = Q\sum_{m=-\infty}^{\infty}\frac{i^m m e^{im\varphi}}{p^2-m^2}J_m(KR)e^{i\,m\frac{\pi}{q}}. \quad (26)$$

Superposition of Eqs. (25) and (26) gives a dipole,

$$|p,-p,\pm\rangle = |p,-p\rangle + |p,-p,q\rangle = Q\sum_{m=-\infty}^{\infty}\frac{i^m m e^{im\varphi}}{p^2-m^2}J_m(KR)\left(1\pm e^{i\,m\frac{\pi}{q}}\right). \quad (27)$$

If $q = 1$ the terms with $m = 2m' + 1$ for a sign (+) vanish while the residual terms form the state

$$|p,2,+\rangle = i4Q \sum_{m=0}^{\infty} (-1)^m \frac{(2m)\,\sin(2m\varphi)}{p^2 - (2m)^2} J_{2m}(KR). \quad (28)$$

In turn, for a sign (−) the terms with $m = 2m'$ vanish and we find the state

$$|p,2,-\rangle = -4Q \sum_{m=0}^{\infty} (-1)^m \frac{[(2m+1)]\sin[(2m+1)\varphi]}{p^2 - [(2m+1)]^2} \times J_{2m+1}(KR). \quad (29)$$

The first state, Eq. (28), does not contain any optical vortices but only the set of edge dislocations of the order $p = 2$ as well as Eq. (29) with $p = 1$.

In order to obtain higher-order beams, e.g., with $p = 4$, we set a phase difference between two dipole states, Eq. (30), equal to $\Delta\varphi_n = \pi$. As a result one obtains

$$|p,4,\pm\rangle = Q \sum_{m=-\infty}^{\infty} (-1)^m \frac{(2m)e^{i2m\varphi}(1 \pm e^{im\pi})}{p^2 - (2m)^2} J_{2m}(KR), \quad (30)$$

so that the two states are

$$|p,4,+\rangle = i2Q \sum_{m=0}^{\infty} (-1)^m \frac{(4m)\sin(4m\varphi)}{p^2 - (4m)^2} J_{4m}(KR) \quad (31)$$

for the sign (+), and

$$|p,4,+\rangle = i2Q \sum_{m=0}^{\infty} (-1)^m \frac{(4m+2)\sin(4m+2)\varphi}{p^2 - (4m+2)^2} J_{4m}(KR) \quad (32)$$

for the sign (−).

By means of such a recurring procedure one obtains the general expressions

$$|p,2s\rangle = i2Q \sum_{m=0}^{\infty} (-1)^m \frac{(4sm)\sin(4sm\varphi)}{p^2 - (4sm)^2} \times J_{4sm}(KR), \quad s = 1,2\ldots, \quad (33)$$

$$|p,2s+1\rangle = -2Q \sum_{m=0}^{\infty} (-1)^m [2s(2m+1)+1] \times \frac{\sin[2s(2m+1)+1]\varphi}{p^2 - [2s(2m+1)+1]^2} J_{2s(2m+1)+1}(KR), \quad (34)$$

where $s = 0, 1, 2\ldots$ is a number of the recurring transformations, whereas $2s$ and $2s + 1$ are topological indices of the wave constructions.

The following step is to rotate the initial dipole through an angle $\varphi_0 = \frac{\pi}{2}$. Such a transformation turns the sine in Eqs. (33) and (34) into the cosine at $m = 0$ at arbitrary index s. As a result we obtain the states with the centered optical vortices

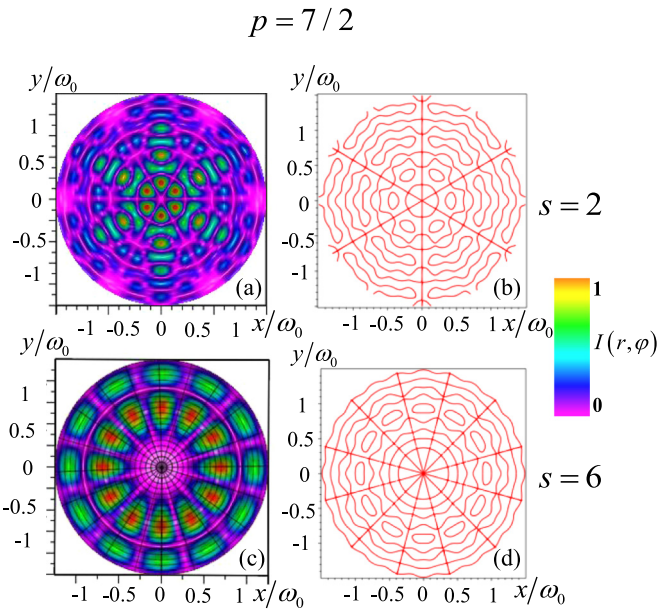

FIG. 4. Intensity distributions $I(r,\varphi)$ (a,c) and lines of the edge dislocations (b,d) of the axially symmetric beams shaped by the fractional-order vortex beams.

of the required integer-order topological charges $l = 2s$ or $l = 2s + 1$,

$$|p, \pm l\rangle = |p,s\rangle_0 \pm i|p,s\rangle_{\pi/2}. \quad (35)$$

Intensity $I(r,\varphi)$ distributions of the axially symmetric fields shown in Figs. 4(a) and 4(c) illustrate the optical constructions built up of the broken fractional vortex beams on the basis of Eqs. (33) and (34). An interesting feature of these structures is that there are no optical vortices in them. Instead we see in Figs. 4(b) and 4(d) the intricate pattern of the degenerated edge dislocations webbing tightly around the beam pattern. Three [see Fig. 4(b)] and six [see Fig. 4(d)] nodal lines (radial edge dislocations) intersect at the axis.

On the other hand, expressions (35) and (36) govern the shaping of the optical vortices shown in Fig. 5. The centered optical vortices with the topological charges $l = 3$ (at the left) and $l = 6$ (from the right) are framed by a necklace of degenerated edge dislocations.

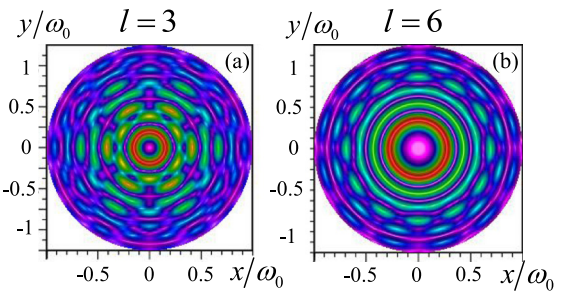

FIG. 5. Intensity beam distributions $I(r,\varphi)$ with the centered propagation-invariant higher-order vortices framed by a necklace of edge dislocations for the $l = 3$ and $l = 6$ topological charges of the centered vortices.

Thus a simple rotation of two topological dipoles through discrete angles (Fig. 3) enables us to form singular beams with the required centered integer-order optical vortices. When propagating, such a complex beam transforms its framing far from the axis while the central part preserves the singular structure.

At the same time, all the beam states (both with the integer-order and fractional-order vortices) in free space or uniform isotropic media are not degenerated; they have different Gouy phases depending on their topological charges m. It is this feature that makes the fractional-order beam scatter over the integer-order vortices forming a complex field distribution under propagation.

We revealed that appropriate compositions of fractional-order beams can preserve their structure (at least near the axis) under propagation. Despite the complex behavior of the fractional vortex beam in free space, the above presented results enable us to originate alternative vortex-beam constructions that can uncover their extraordinary properties in a nonuniform anisotropic media as we will see later.

However, the exclusion is the Γ-G vector beams that can either break down the fractional vortex into a set of integer-order vortices or, vice versa, assemble them into one fractional vortex at the far diffraction zone. The control for these opposing processes brings into effect the modulation of the beam parameter K.

Further, we consider two examples of the possible manifestations of the fractional-order vortex beams in the uniform and nonuniform anisotropic media with the distinctive intrinsic symmetry.

III. CONICAL REFRACTION IN BIAXIAL CRYSTALS

A. General remarks

The fractional-charged beams propagating in uniaxial crystals have been partially considered in Ref. [26] for the vortex beams in states $|\pm 1/2\rangle$ (the so-called erf-G beams). Authors showed conversion between the states $|\pm 1/2\rangle \rightleftarrows |1/2 \pm 2\rangle$ in circular polarized components. It is easy to generalize this rule to arbitrary states $|p\rangle \rightleftarrows |p \pm 2\rangle$. However, fractional-order vortices are not degenerated in the Gouy phases and are scattered over all possible states of integer-order vortices.

At the same time, biaxial crystals have one interesting type of dielectric tensor property that yields a singularity of wave normals—Hamilton's diabolical point [28]—that induces a space-variant birefringence with typical distribution of birefringent axes [see Fig. 6(b)]. The fact is that there are two types of waves in a biaxial crystal with wave-front braches of slow (s) and fast (f) velocity as is shown in Fig. 6(a). The wave fronts intersect each other at four points (e.g., the point *DP*) defining two directions of optical axes. The wave surfaces at the vicinity of the point *DP* take the form of a double wave cone that looks like a "diabolo" [28]. According to Hamilton the normals to the wave surface are not defined at the *DP* point but originate, in turn, a new cone of the energy flux—the ray cone [see the callout in Fig. 6(a)]. The singular point *DP* was called the diabolical point (the detailed review is presented in the papers [28,29], and references therein). As a result an optical beam propagating along one

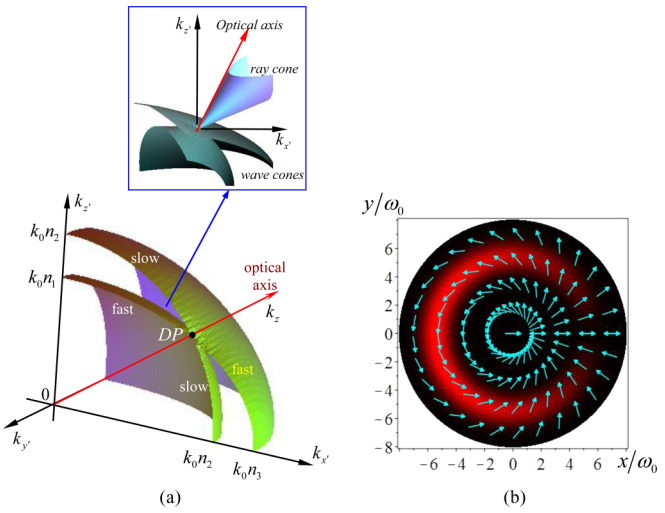

FIG. 6. (a) The shaping of a diabolic point (DP) in a biaxial crystal as intersection of two wave surfaces. The callout illustrates places of the ray and wave cones of the conical refraction (b) Space-variant directions of the biaxial crystal birefringence under the conditions of the conical refraction on the background of the beam intensity.

of the crystal's optical axes transforms into a conical one inside the crystal. The phenomenon was called the conical refraction. The initial circular polarization of the beam splits into a cone of local linear polarizations in such a way that the electric vector **E** rotates though an angle π after a full path tracing around the cone's axis as shown in Fig. 6(b). Generalization of Hamilton's approach onto Gaussian beams introduces corrections into the propagation and distribution of the field [28]. This phenomenon is called the conical diffraction. The conical form of the beam suggested the solutions of the problem in the form of Bessel beams. At the same time, the polarization distribution in Fig. 6 has also much in common with that of erf−G and Γ-G beams in Fig. 4 [17]. Little misalignments of the field patterns far from the optical axis are due to a complex structure of the fractional-charged vortex beams.

The results presented in the papers [29–32] have shown that the uniaxial crystal exhibits a tendency to turn into a biaxial one after its twisting around the optical axis. The space-variant symmetric field of TE or TM eigenmodes inherent to a uniaxial crystal [33] at the initial plane $z = 0$ transforms into the asymmetric field distribution similar to that shown in Fig. 6. In contrast to the standard conical diffraction in the typical biaxial crystals, the intensity distribution in the twisted uniaxial crystal has not the pronounced C-shaped form or the circular form with Poggendorff rings [29] but the pattern gets smeared over the cross section with a singular point at the axis. Nevertheless, the fine structure of the pattern can be controlled by means of either mechanical or electrical devices.

The presented results point out the fact that eigenmode beams of the conical diffraction and adjoining phenomena are worth searching for among the fractional-order vortex-beams. Thus the aim of the following subsection is to study the propagation and conversion of the fractional-order vortex beams of the Bessel type along one of the optical axes of the biaxial crystal. We will focus our attention on the

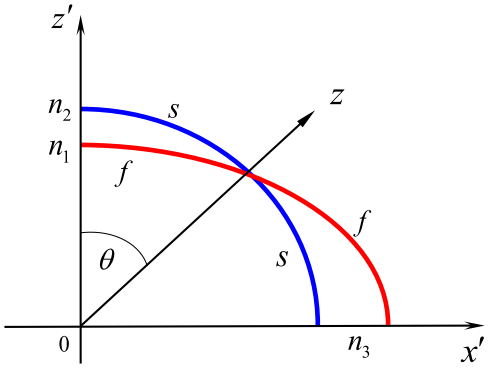

FIG. 7. Sketch of the surface of normals of the slow (s) and fast (f) wave fronts in the optical axis direction. The crystal optical axis is directed along the z axis.

following question: Could the input field with a space-variant polarization identical to that of the crystal birefringence in Fig. 6 (say, the state $|p\rangle$) propagate without structural perturbation? If yes, then we can expect the fractional-order mode beam to be an eigenmode of the medium.

B. Theoretical treatment

The underlying idea of our treatment is grounded on the constitutive papers [34–37] where the authors consider evolution of the electric field **E** (rather than the electric displacement **D**) of Bessel beams in biaxial crystals under the condition of conical diffraction. The fact is that in a biaxial crystal the wave normal is not directed along the beam propagation so that there appear additional terms in the vector wave equation because of changes in the permittivity tensor. In our case we can use this tensor in the form [37]

$$\hat{\varepsilon} = \begin{pmatrix} \varepsilon_a & 0 & -\varepsilon_{13} \\ 0 & \varepsilon_2 & 0 \\ -\varepsilon_{13} & 0 & \varepsilon_b \end{pmatrix}, \tag{36}$$

where $\varepsilon_a = \varepsilon_1 + \varepsilon_3 - \varepsilon_1\varepsilon_3/\varepsilon_2$, $\varepsilon_b = \varepsilon_1\varepsilon_3/\varepsilon_2$, $\varepsilon_{13} = \sqrt{\varepsilon_1\varepsilon_3(\varepsilon_2-\varepsilon_1)(\varepsilon_3-\varepsilon_2)}/\varepsilon_2$, $n_1^2 = \varepsilon_1$, $n_2^2 = \varepsilon_2$, $n_3^2 = \varepsilon_3$ are the principal refractive indices of the crystal along the axes x', y', z'.

The optical axis directed at the angle θ to the axis z' $\tan\theta = \sqrt{\frac{\varepsilon_3(\varepsilon_2-\varepsilon_1)}{\varepsilon_1(\varepsilon_3-\varepsilon_2)}}$, $\varepsilon_1 < \varepsilon_2 < \varepsilon_3$ passes through a diabolical point where slow (s) and fast (f) wave fronts are tangent to each other as shown in Fig. 7.

The authors of the papers [35,38] showed that the circularly polarized beam components with the spectral function at the crystal input $A(k_\perp)$ ($k_\perp$ is the transverse wave number of the initial beam), are

$$E_+(r,\varphi,z) = \sum_{m'=-\infty}^{\infty} e^{im'\varphi} \int i^{m'} k_\perp A_{m'}(k_\perp) J_{m'}(k_\perp r) \times \exp\left(-i\frac{k_\perp^2}{2k_b}z\right)\cos(\gamma_0 k_\perp z) dk_\perp e^{i\beta z},$$

$$E_-(r,\varphi,z) = -\sum_{m'=-\infty}^{\infty} i^{m'} e^{i(m'+1)\varphi} \int k_\perp A_{m'}(k_\perp) J_{m'+1}(k_\perp r) \times \exp\left(-i\frac{k_\perp^2}{2k_b}z\right)\sin(\gamma_0 k_\perp z) dk_\perp e^{i\beta z}. \tag{37}$$

It means that the right-hand circularly polarized beam bearing a series of the vortex beams of the mth order and a complex angular spectral distribution $A(k_\perp)$ at the crystal input excites a series of vortex beams of the $(m+1)$th order with the same angular spectrum $A(k_\perp)$ in the left-hand circularly polarized component.

Similarly, it can be shown that the composition of the vortex beams of the $(m+1)$th order with the spectral distribution $A(k_\perp)$ in the left circularly polarized component at the crystal input excites a series of vortex beams of the mth order with the same angular spectrum $A(k_\perp)$ in the right-hand circularly polarized component, i.e.,

$$E_+(r,\varphi,z) = \sum_{m'=-\infty}^{\infty} e^{im'\varphi} i^{m'} \int k_\perp A_{m'}(k_\perp) J_{m'}(k_\perp r) \exp\left(-i\frac{k_\perp^2}{2k_b}z\right)\sin(\gamma_0 k_\perp z) dk_\perp e^{i\beta z},$$

$$E_-(r,\varphi,z) = \sum_{m'=-\infty}^{\infty} i^{m'} e^{i(m'+1)\varphi} \int k_\perp A_{m'}(k_\perp) J_{m'+1}(k_\perp r) \exp\left(-i\frac{k_\perp^2}{2k_b}z\right)\cos(\gamma_0 k_\perp z) dk_\perp e^{i\beta z}. \tag{38}$$

The circularly polarized single Bessel beam $E_+^{in} = J_m(k_\perp r)\exp(im\varphi)e^{i k_z z}$ with an integer-order topological charge m, directed along the crystal optical axis (axis z in Fig. 7), has the conical spectral distribution $A(k_\perp = k_\perp^{(0)}) = \text{const}$. In order to obtain the beam propagation of such a beam it is sufficient to multiply Eq. (37) by the factor $\delta(k_\perp - k_\perp^{(0)})$, and making the substitution $m' \to m$ we find

$$\mathbf{E}_1 = \begin{pmatrix} E_+ \\ E_- \end{pmatrix} = \begin{pmatrix} J_m(k_\perp r)\exp(im\varphi)\cos(\gamma_0 k_\perp z) \\ -J_{m+1}(k_\perp r)\exp[i(m+1)\varphi]\sin(\gamma_0 k_\perp z) \end{pmatrix} \exp\left(-i\frac{k_\perp^2}{2k_b}z\right)e^{i\beta z}, \tag{39}$$

where $\beta = n_2 z$, $k_b = k n_2/2(1+\varepsilon_2/\varepsilon_b)$, $\gamma_0 = \varepsilon_{13}/2\varepsilon_b$.

Similar to that we can obtain from Eq. (38) for the initial field in the form $E_{-}^{in} = -J_{m+1}(k_\perp r)\exp[i(m+1)\varphi]e^{i\,k_z z}$ the expression

$$\mathbf{E}_2 = \begin{pmatrix} E_+ \\ E_- \end{pmatrix} = \begin{pmatrix} J_m(k_\perp r)\,\exp(im\varphi)\,\sin(\gamma_0 k_\perp z) \\ J_{m+1}(k_\perp r)\,\exp[i(m+1)\varphi]\cos(\gamma_0 k_\perp z) \end{pmatrix} \exp\left(-i\frac{k_\perp^2}{2k_b}z\right)e^{i\beta z}. \tag{40}$$

Combination $\mathbf{E}_1 \pm i\mathbf{E}_2$ of Eqs. (39) and (40) gives

$$\mathbf{E} = \frac{1}{2}\begin{pmatrix} J_m(k_\perp r)\,\exp(im\varphi) \\ J_{m+1}(k_\perp r)\,\exp\left[i(m+1)\varphi - i\frac{\pi}{2}\right] \end{pmatrix} e^{i\,(\frac{k_\perp^2}{2k_b}+\gamma_0 k_\perp+\beta)z} \tag{41}$$

and

$$\mathbf{E} = \frac{1}{2}\begin{pmatrix} J_m(k_\perp r)\exp(im\varphi) \\ J_{m+1}(k_\perp r)\exp\left[i(m+1)\varphi + \frac{\pi}{2}\right] \end{pmatrix} e^{i\,(\frac{k_\perp^2}{2k_b}-\gamma_0 k_\perp+\beta)z}. \tag{42}$$

Equations (41) and (42) show that such fields with space-variant polarization can propagate through the crystal without any structural transformations but with different propagation constants $\beta_\pm = \frac{k_\perp^2}{2k_b} \pm \gamma_0 k_\perp + \beta$.

The polarization distribution in the mode beam cross section in Eq. (41) has a complex form in contrast to that of the standard structure shown in Fig. 6. Figure 8 illustrates typical space-variant polarization for the mode index $m = 6$. Directions of the polarization ellipse's axes ψ are depicted on the background of the mode intensity distribution. The ellipticity states specified by the Stokes parameter S_3 as a function of radial position [see Fig. 8(b)] oscillate from right circularly polarized $S_3 = 1$ to left circularly polarized $S_3 = -1$ states. However, the ellipticity S_3 preserves its value along the azimuth direction. Although the path tracing around the beam axis through an angle $\varphi = \pi$ is accompanied by the ellipse rotation through an angle $\psi = \pi/2$, the full path tracing results in reinstating both the polarization state and the beam phase. Such a space-variant polarization of the eigenmode manifests itself in the ring pattern of intensity distribution while the linear space-variant polarization is in line with C-shaped distribution in Fig. 6.

Note that the propagation constants $\beta_\pm$ do not depend on the vortex topological charge m. Thus we can write the solution for a fractional-order vortex beam as a superposition of partial solutions in Eq. (41) with the spectral vortex density $\rho(p) = (p-m)^{-1}$ [see Eq. (8)] in the form

$$\begin{aligned}\mathbf{E}_p^{(+)} &= c_p \begin{Bmatrix} \sum_{m=-\infty}^{\infty} \frac{i^m J_m(k_\perp r)\exp(im\varphi)}{p-m} \\ -\sum_{m=-\infty}^{\infty} \frac{i^{m+1} J_{m+1}(k_\perp r)\exp[i(m+1)\varphi]}{p-m} \end{Bmatrix} e^{i\beta_+ z}, \\ &= c_p \begin{Bmatrix} \sum_{m=-\infty}^{\infty} \frac{i^m J_m(k_\perp r)\exp(im\varphi)}{p-m} \\ -\sum_{m=-\infty}^{\infty} \frac{i^{m+1} J_{m+1}(k_\perp r)\exp[i(m+1)\varphi]}{p+1-(m+1)} \end{Bmatrix} e^{i\beta_+ z} \\ &= \begin{pmatrix} |p\rangle \\ -c_{p+1}|p+1\rangle \end{pmatrix} \exp(-i\beta_+ z), \end{aligned} \tag{43}$$

where $c_p = \sin\pi p e^{ip\pi}$. Similar to that we can write down the mode field $\mathbf{E}_p^{(-)}$ with the propagation constant β_-:

$$\mathbf{E}_p^{(-)} = \begin{pmatrix} |p\rangle \\ ic_{p+1}|p+1\rangle \end{pmatrix} \exp(-i\beta_- z), \tag{44}$$

with $\beta_\pm = \frac{k_\perp^2}{2k_b} \pm \gamma_{in} k_\perp - \beta$.

Typical field distributions on the background of the beam intensity are shown in Fig. 9 for $|0.5\rangle$ and $|7.5\rangle$ fractional states. For the computer simulation we chose the potassium gadolinium tungstate $KGd[WO_4]_2$ (KGW) biaxial crystal

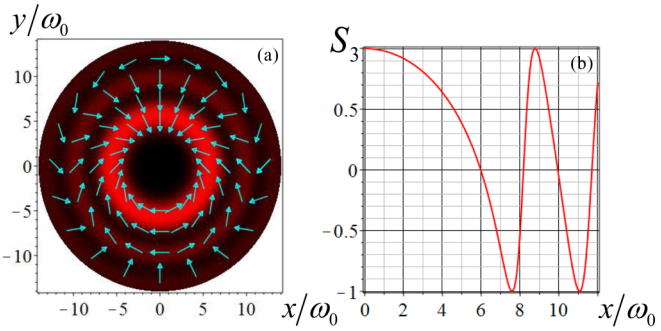

FIG. 8. The polarization state distribution of the mode beam with the index $m = 6$ (a), and (b) the dependence of the ellipticity degree $S_3(r)$ on the beam radius r.

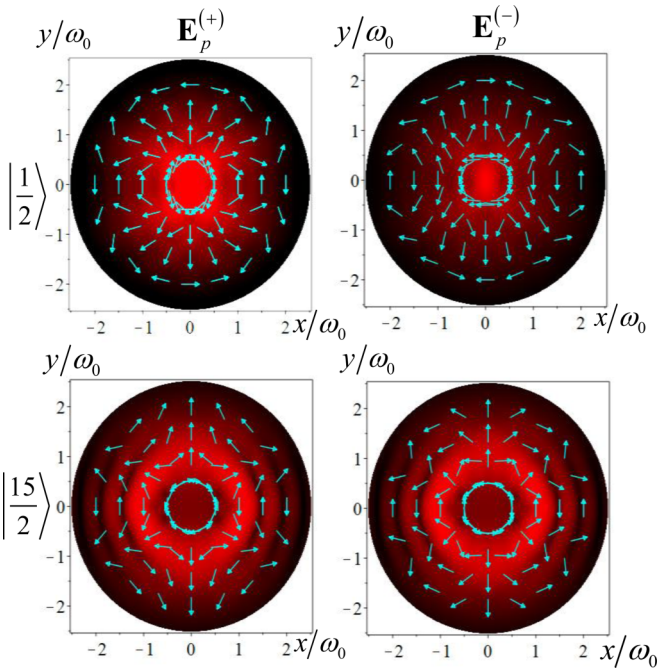

FIG. 9. Field distributions of the fractional-order vortex beam in the potassium gadolinium tungstate KGW biaxial crystal.

with refractive indices $n_1 = 2.013, n_2 = 2{,}045, n_3 = 2.086$, for the wavelength $\lambda = 0.63\,\mu$m, so that the crystal and beam control parameters are $\gamma_{in} \approx 0.0087$ rad, $\varepsilon_b \approx 4.224$, and $k_\perp \approx 1.74 \times 10^5\,\mathrm{m}^{-1}$.

When the initial beam at the initial plane $z = 0$ is right-hand circularly polarized, the field of the conical diffraction is defined by a combination of the eigenstates Eqs. (43) and (44),

$$\mathbf{E} = \begin{pmatrix} |p\rangle \cos(\gamma_0 k_\perp z) \\ i c_{p+1} |p+1\rangle \sin(\gamma_0 k_\perp z) \end{pmatrix} \exp(-i\bar{\beta} z). \tag{45}$$

where $c_{p+1} = \sin p\pi / \sin(p+1)\pi$. As a result we observe the beating between the field components. The beat length in our case equals $L_B = 2\pi/(\gamma_{in} k_\perp) \approx 4.15$ mm. It means that the states $|p\rangle$ and $|p+1\rangle$ appear alternately at this length while the eigenmode states Eqs. (43) and (44) in Fig. 9 emerge at the lengths $L_{e,o} = \pi(2n+1)/(4\gamma_{in} k_\perp)$, $n = 0,1,2\ldots$.

In contrast to the integer-order vortex beams (see Fig. 8), an azimuthal angle of the linear polarization ψ of the fractional-order states in Fig. 9 has a complex distribution over the beam cross section depending on both the topological charge p and the transverse coordinate r. In addition, we found that the greater the value of the parameter $k_\perp$ the greater the number of polarization variations along the radial direction $\hat{\mathbf{r}}$.

Thus the right-hand circularly polarized Bessel beam with the p fractional-order vortex at the crystal input induces the beam with $p+1$ fractional-order vortex at the left-hand circular polarization at some crystal length. At the beam length $z = \frac{\pi}{2\gamma k_\perp}(2n+1)$, $n = 0,1,2\ldots$ energy is concentrated in the $|p+1\rangle$ state. However, the eigenmodes $\mathbf{E}_p^{(\pm)}$ for different charges p have the same propagation constants (i.e., are degenerated over p). Any superposition of the fractional-order vortex beams obeys the same transformations Eq. (45) as the single field states.

Thus during the conical diffraction process the energy transports from the E_+ component with a fractional topological charge p into the E_- component with a charge $p+1$ and vice versa for wide types of the field structure of fractional-order vortex beams. Since for simplicity we consider Bessel beams without a Gaussian envelope, the fractional-order beam maintains its structure under propagation for all the values of p. The real BG beams with integer-order vortices have a very cumbersome mathematical representation [38] and we kept them out of our consideration. However, each BG beam in the crystal gets its own Gouy phase under propagation that depends on the topological charge m. It means that the fractional-order vortex fields as a combination of integer-order beams are unstable structures in biaxial crystals.

IV. NONUNIFORM BIREFRINGENT MEDIA

A. Space-variant unbounded birefringent medium

The brightest representatives of the space-variant media are the so-called q plates [39]. The q plate is, in the first version, a slab of a uniform birefringent medium (liquid crystal) with different local directions of the crystal birefringence while the slab has uniform phase retardation. The space-variant birefringence of the q plates is set by the topological charge q imprinted in the q plate. This imprinted charge is equal to the number of rotations of the optical axis in a path circling around the q plate's center. Obviously, the value of q can be integer or half integer. The q value can be controlled either mechanically or electrically [40,41]. The beam turns into a new wave state due to superimposing of a great number of plane waves with different polarization states. In that regard, the processes of the conical diffraction in the uniform biaxial crystal should not much differ from the effect of the q plate. Thus there is no appropriate physical mechanism in such media that could ensure creation of a propagation-invariant fractional vortex beam. These optical systems change only the field's OAM.

At first sight it could have seemed that the only physical mechanism of shaping the beams with the space-variant polarization in a medium is in superimposing the uniform propagating waves. However, the Fourier synthesis is a proper approach only for unbounded media. Meanwhile, for the media with boundary surfaces where along with propagating waves the nonradiative (evanescent [42]) waves may also exist, such an approach involves certain mathematical difficulties, which make it unfavorable. In particular, such is the case of the paraxial propagation.

One of such media are the photonic crystal fibers that represent tightly compressed arrays of optical fibers. Their total birefringence is determined by the structure of the fiber's stacking and their local properties [43–45]. The photonic crystal fibers have two indefeasible advantages: the wave guiding property and the controlled fiber coupling. The simplest model of the photonic crystal fiber is a circular fiber array [46]. In the following section we will try to uncover the basic physical processes responsible for the structural stability of vortex constructions with half-integer topological charges in a circular fiber array with a discrete space-variant birefringence.

B. Anisotropic fiber array: nonadiabatic following and optical quarks

1. *Supermodes of anisotropic arrays*

We will focus our attention on the discrete system of single mode birefringent fibers inserted into a transparent *continuous* medium with a uniform refractive index n_{cl} less than that of the fiber core $n_{co} < n_{cl}$ [21,46–48]. Each optical fiber is located at the vertices of a regular N-gon as shown in Fig. 10. We will assume that the principal birefringence refractive indices n_e and n_o are such that $n_e \approx n_o \approx n_{co}$, $\delta n = n_{co} - n_{cl} \ll 1$, and $\Delta n = n_e - n_o \ll \delta n$.

The principal point of our consideration is a distinctive distribution of the axes' birefringence over the optical fibers: the birefringence directions at the jth fiber make an angle γ_j^p with the X axis of the global frame,

$$\gamma_j^p = \frac{2\pi p j}{N} = 2\varphi_p j, \quad \varphi_p = \frac{\pi}{N} p, \tag{46}$$

where $j = 0,1,2\ldots N-1$ and p is a number of rotations of the fiber birefringence axis; i.e., the index p controls the position of the director of the anisotropic medium. The index $p = (2n_p + 1)/2$, $n_p = 0,1,2\ldots$ sets the characteristic index of the fiber array. The angle φ_j points out the position of the local fiber in the array. In addition, our consideration is restricted to the case of even N.

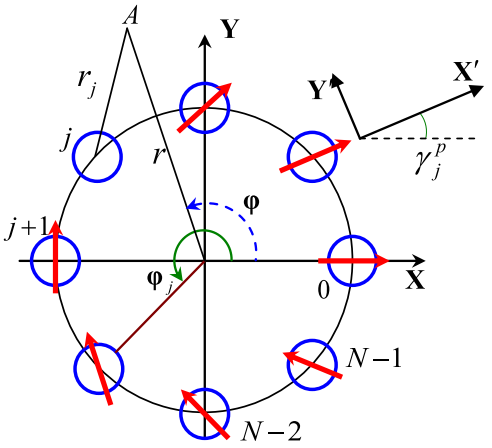

FIG. 10. Sketch of the birefringent fiber positions in the fiber array. Arrows inside circles are directed along the fiber birefringent axis.

The fibers in the array are coupled due to a mutual penetration of the guided fields inside neighboring fibers. The coupling coefficient a (with the dimension m^{-2}) is general for all arrays and depends on the radius of the core. As a result the coupled fiber modes form stable phase-locked field combinations (so-called supermodes) propagating with certain propagation constants. The field structure and the spectrum of their propagation constants are determined by the perturbation matrix [46]:

$$\hat{P} = a\cos 2\varphi_p \begin{pmatrix} 0 & 1 & 0 & \cdots & 0 & -1 \\ 1 & 0 & 1 & 0 & \cdots & 0 \\ 0 & 1 & 0 & \cdots & 0 & \cdots \\ \cdots & 0 & \cdots & \cdots & 1 & 0 \\ 0 & \cdots & 0 & 1 & 0 & 1 \\ -1 & 0 & \cdots & 0 & 1 & 0 \end{pmatrix}, \quad (47)$$

built through averaging of a certain operator over X',Y'-polarized fundamental modes located at individual fibers. The mode spectrum P_v is found from the eigenvalue equation,

$$\hat{P}\mathbf{K}_v = P_v\mathbf{K}_v. \quad (48)$$

For the components K_v^j of the eigenvector $\mathbf{K}_v$ one has the following solution:

$$K_v^j = \frac{\varepsilon^j}{\sqrt{N}}\exp(ij\varphi_{2m+1}). \quad (49)$$

The composite index v in Eq. (49) consists of two elements $v = (\varepsilon,m)$ so that its first element assumes two values: $\varepsilon = \pm 1$, $m = 0,1\ldots N/2-1$ and the eigenvalue reads as

$$P_v = \varepsilon a\cos 2\varphi_p\cos\varphi_{2m+1}. \quad (50)$$

The expressions for supermodes are built on the basis of the components K_v^j and are given by

$$\mathbf{X}_v = \sum_{j=0}^{N-1} K_v^j\tilde{G}_j\mathbf{i}'_j, \quad \mathbf{Y}_v = \sum_{j=0}^{N-1} K_v^j\tilde{G}_j\mathbf{j}'_j, \quad (51)$$

where $\mathbf{i}'_j$, $\mathbf{j}'_j$ are the unit vectors directed along the X',Y' axes associated with the j fiber. For the radial function we chose the Gaussian approximation [36],

$$\tilde{G}_j = E\exp\left(-\frac{r_j^2}{2w^2}\right), \quad (52)$$

where E is the field amplitude, $w = \rho_0/\sqrt{2\ln V}$, ρ_0 is the radius of the fiber core, and $V = k\rho_0\sqrt{2\delta n}$.

The supermodes, Eq. (51), are formed of fundamental modes of local fibers polarized along the X',Y' local axes. The propagation constant $\beta_v^{x,y}$ of the $\mathbf{X}_v,\mathbf{Y}_v$ supermodes is given by [6]

$$\beta_v^{x,y} = \bar{\beta} + \frac{P_v}{2\bar{\beta}} \pm k\Delta n, \quad (53)$$

where $\bar{\beta}$ stands for the scalar propagation constant of each local fiber and the upper sign relates to β_v^x.

2. Optical quarks

It is convenient to analyze the structure of supermodes, Eq. (51), in the circularly polarized basis. The contributions to the jth local fiber in the right-hand circular component are modulated at the vertices by the phase factor $\exp[i2\pi j(m-n_p)/N]$ and in the left-hand component by the $\exp[i2\pi j(m+n_p+1)/N]$ factor. When we consider the array as a whole, the j index changes from 0 to $N-1$ so that the total increments of the phases over the vertices of the array are $2\pi(m-n_p)$ and $2\pi(m+n_p+1)$. As we have in detail shown in Ref. [47], these increments in orthogonal circular polarizations set *integer-order* charges of discrete vortices in the fiber array. At first sight it seems that we can conclude that such fiber array *cannot* support the propagation of vortex modes with the fractional-order topological charges. However, we have shown in Sec. IV A that fractional-order vortices can be formed through superimposing the integer-order vortex modes (although they are unstable). It proves it is also possible to form from the supermodes, Eq. (49), their combinations that explicitly contain, in the circularly polarized components, the fractional-order vortices.

The basic point of our consideration lies in choosing the eigenmodes bearing the fractional-order vortices. We can reach the desired results through combining the degenerated modes of the fiber array. In fact, the eigenvalues of the matrix $\hat{P}$, Eq. (47), are double degenerate because $P_{\varepsilon,m} = P_{-\varepsilon,N-2-m-1}$ [see Eq. (50)]. Since $\mathbf{K}^*_{\varepsilon,m} = \mathbf{K}_{-\varepsilon,N/2-m-1}$ it follows that $\mathbf{K}^*_v$ belongs to the same eigenvalue as $\mathbf{K}_v$. Further we have $(\mathbf{K}^*_v\cdot\mathbf{K}_v) = 0$; i.e., these vectors are linearly independent. Thus we choose a new set of eigenvectors in the form

$$\mathbf{e}_1 = \frac{\mathbf{K}_v - \mathbf{K}^*_v}{2i}, \quad \mathbf{e}_{-1} = \frac{\mathbf{K}_v + \mathbf{K}^*_v}{2}. \quad (54)$$

The new set of the eigenvectors can be conventionally divided into two parts: with $s = +1$ ($\mathbf{e}_{+1}$ eigenvector) and $\varepsilon = -1$ ($\mathbf{e}_{-1}$ ones). In accordance with Eq. (47) we can obtain the alternative representation of the eigenvector components,

$$\Gamma_v^j = \frac{1}{\sqrt{N}}\begin{cases}\sin(j\varphi_{2m+1}), & \varepsilon = 1,\\ \varepsilon^j\cos(j\varphi_{2m+1}), & \varepsilon = -1,\end{cases} \quad (55)$$

while the spectrum of the propagation constants remains intact and is defined by Eq. (50). The new set of eigenvectors is

recovered from Eq. (51) by the replacement $K_v^j \to \Gamma_v^j$. We will call the fields with $\varepsilon = 1$ and $\varepsilon = -1$ the odd $\mathbf{E}_{o,m}$ and the even $\mathbf{E}_{e,m}$ mode beams, respectively.

For example, at $\varepsilon = 1$ for the amplitudes at the jth fiber for circular components of the $\tilde{\mathbf{X}}_v$ supermode we obtain $\exp(-2i\varphi_p j)\sin(\varphi_{2m+1} j)$ in the right circular polarization and $\exp(2i\varphi_p j)\sin(\varphi_{2m+1} j)$ in the left-hand component. For the case $\varepsilon = -1$, the sines should be replaced by cosines multiplied by the factor ε^{j-1}. In this case the total phase increments in the components over the vertices of the array are $\mp 2\pi p$. In fact, the birefringence pattern of the fiber array inserts the fractional-order topological charges p into supermode fields.

Since a stable supermode $\tilde{\mathbf{X}}_v$ turns out to be composed of unstable fractional topological charges of opposite values nested in orthogonal polarizations, one can regard such a state as composed of *optical quarks* (predicted in [49]) similar to that in the Standard Model of particle physics, in particular, in the Gell-Mann quark model of the hadrons [50]. (By convention, we apply the term "optical quark" only to the vector supermode rather than to its components.) The optical quarks can exist in coupled states only inside the media with the inherent symmetry of the permittivity tensor. Outside the medium the optical quark pairs break up into a set of the guided modes of the outer optical structure.

To study the properties of optical quarks, we use the expressions for the electric field components $E_v^{\pm}$ of the supermodes [17]:

$$E_v^{\pm}(r,\varphi,z) = G\sqrt{N}\sum_{j=0}^{N-1}\Gamma_v^j \exp \times\left[\frac{rr_0}{w^2}\cos(\varphi - 2\varphi_j) \mp 2ip\varphi_j - i\beta_v z\right], \quad (56)$$

where $G = E\exp[-(r^2 + r_0^2)/(2w^2)]$; r_0 is the array radius. Typical field patterns on the background of the intensity distributions of the supermodes are shown in Fig. 11. The pattern in Fig. 11(a) has the C-shaped form, where the electric field is directed along the $\mathbf{X}'$ direction of the birefringence axis in each local fiber (see also Fig. 10). In the pattern in Fig. 11(b) the intensity distribution is the mirror-reflected intensity in Fig. 11(a). However, the electric fields in each local fiber are directed along the $\mathbf{Y}'$ under the condition that the fiber array index p remains the same (the local birefringent directions do not change). In accordance with Eq. (53) the propagation constants differ from each other by the value $\Delta\beta = \beta_1 - \beta_{-1} = 2k\Delta n$ [see Eq. (53)]. The patterns in Figs. 11(c) and 11(d) have the mirror-reflected positions of the field zeros ($m = 1$) but the fields in each local fiber are directed along the $\mathbf{X}'$ axes, correspondingly.

One should note that the point $x = y = 0$, around which the full path tracing is carried out, is not a singular point in any sense. The fact is that although the field has a space-variant linear polarization over all cross sections, the central point $x = y = 0$ cannot be related to any well-known polarization singularities. Typical polarization singularities [star, lemon, or (le)monstar] imply the presence of the circular polarization at the center [51], whereas supermodes are locally

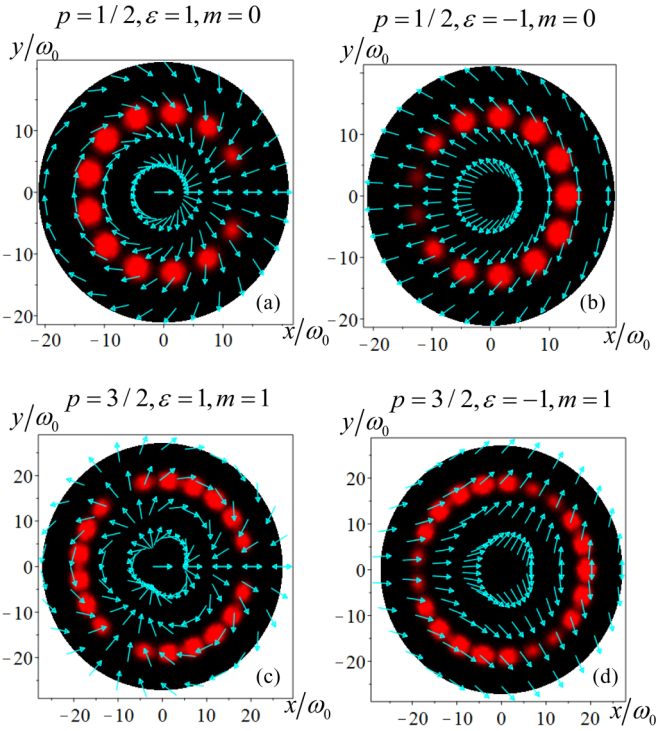

FIG. 11. The intensity $I(r,\varphi)$ and polarization distributions for the supermodes with different parameters p and ε.

linearly polarized. Indeed, since $E_v^+ = (E_v^-)^*$, the third Stokes parameter $S_3 = |E_v^+|^2 - |E_v^-|^2 = 0$ proves this statement.

The following point of our consideration is to study the phase structure in the components of the fractional-order vortex mode. Figure 12 shows the phase patterns plotted on the basis of Eq. (56) for the components of the vortex beams. One observes the ladderlike structure of the phase for the topological charges $p = \pm 1/2$ for even and odd field components where the phase jump $\Delta\Phi = \pi$ is present at the cut plane $\varphi = 0$. In Sec. II A we argued that the fractional-order vortex in the beam components can be composed of an infinite sum of the integer-order ones. The situation in the array in question seemingly illustrates this general statement. However, there is a subtlety to it. Indeed, here we compose a mode with the opposite fractional charges in the components from

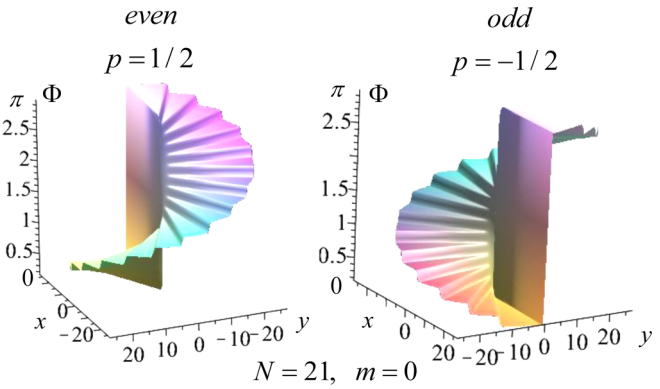

FIG. 12. The ladderlike phase patterns of the supermodes phase Φ with $p = \pm 1/2$.

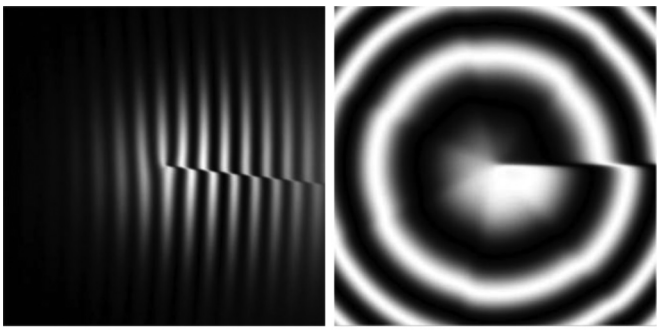

(a) (b)

FIG. 13. The interferential patterns of the $E^{+}_{o,0}$ component with $p = 1/2$.

the modes that bear different integer charges in orthogonal components, whose values are rigidly correlated. In this situation it is not merely a question of Fourier decomposition of fractional-charged scalar fields over integer-charged optical vortices. Should the charges in the mode components be correlated in a fashion other than prescribed by Eq. (49), it would have been impossible to form from them fractional-order vortex modes in the simple manner implied by Eq. (54). We believe that, generally, this is impossible.

The obtained phase diagram shows no integer-charged vortices in the components of the fractional-charged supermodes described by Eq. (56). However, there is a possibility that the presented plotting is too crude a tool to reveal the "hidden vortices." To answer this question and analyze the fine phase structure we studied the interference of the fractional beam with the plane and spherical waves. The interference patterns in Fig. 13 are formed by the superposition of the odd $E^{+}_{o,0}$ component with the topological charge $p = 1/2$ and the plane (a) and spherical (b) waves. We observe the pattern that implies a steplike behavior of the phase. There is only one broken fork at the end of the cut of the interference fringes [see Fig. 13(a)] and the cut of the interference spiral [see Figs. 13(a) and 13(b)] attesting to the phase jump π in the phase structure. This indicates the presence of half-charged vortex nested in the field component. There are no any integer-order vortices in the patterns. Such phase distribution preserves its structure when propagating along the fiber array in contrast to the fractional-order vortex in free space that decays into an infinite number of integer-order vortices [10].

Although the aforementioned results give substantial arguments in favor of the absence of phase singularities in the components of the fractional charge bearing supermodes, it is possible to provide a rigorous analytical proof of this statement. To this end let us introduce an auxiliary mathematical construction known as the scalar optical current. This quantity can be defined for a scalar field Ψ [52] as followd:

$$\mathbf{J} = i(\Psi \nabla_{\perp} \Psi^{*} - \Psi^{*} \nabla_{\perp} \Psi). \tag{57}$$

As such scalar field one can choose any of the circular components, Eq. (56). For a true scalar field the current $\mathbf{J}$ describes the energy density flow [as in the case of quantum mechanics; the current equation (57) is introduced by way of analogy]. In our case this vector has nothing to do with the energy flow of the vectorial electromagnetic field described by

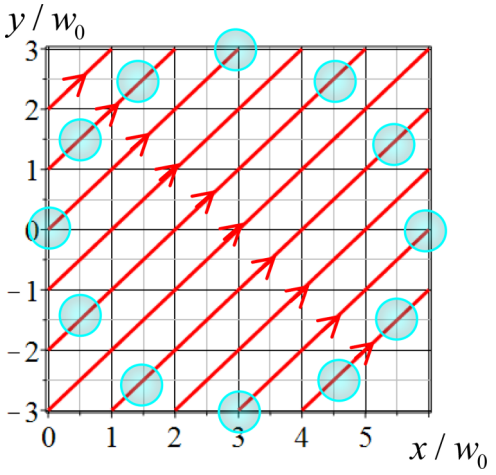

FIG. 14. Streamlines of the optical current on the background of the fiber array $N = 12$. Circles show the fiber positions.

the Poynting vector. We employ this quantity just to study the structure of phase singularities in the components. The current vector $\mathbf{J}$ is helpful while searching for phase singularities because in their vicinities it forms closed trajectories [52]. Taking into account Eqs. (56) and (57), one can obtain the expression for the components of the current vector in the E^{-}_{v} component:

$$J_x = G^2 N \sum_{n,m=0}^{N-1} \exp\left[\frac{r r_0}{w^2}\{\cos(\varphi - \varphi_n) + \cos(\varphi - \varphi_m)\}\right] \times \sin[p(\varphi_n - \varphi_m)]\left(\frac{r_0}{w^2}\cos\varphi_m - \frac{x}{w^2}\right)\sin\varphi_n \sin\varphi_m,$$

and

$$J_y = G^2 N \sum_{n,m=0}^{N-1} \exp\left[\frac{r r_0}{w^2}\{\cos(\varphi - \varphi_n) + \cos(\varphi - \varphi_m)\}\right] \times \sin[p(\varphi_n - \varphi_m)]\left(\frac{r_0}{w^2}\cos\varphi_m - \frac{y}{w^2}\right)\sin\varphi_n \sin\varphi_m.$$

The correspondent current lines are shown in Fig. 14. As is seen, the picture of current flow turns out to be quite unexpectedly simple. The correctness of this numerical result can be confirmed by an analytical consideration. Indeed, for the difference between the transverse components of the current vector $\mathbf{J}$ one can obtain the following expression:

$$J_x - J_y \propto \sum_{n,m=0}^{N-1} \exp[2 r r_0 \cos(\varphi - \varphi_{m+n}) \cos(\varphi_{m-n})/w^2] \times \sin(2p\varphi_{m-n}) \sin\varphi_n \sin\varphi_m. \tag{58}$$

Noting that the summed expression is a convolution of symmetric and antisymmetric (in m and n indices) tensors, one can infer that the right-hand side of Eq. (58) is zero, which gives $J_x = J_y$ that confirms the numerical result. In this way, the current vector in each point of the transverse cross section makes an angle of $\pi/4$ with the coordinate axes. The optical current lines are the set of parallel lines, which cannot contain any closed loops, which are the indicators of phase

singularities. Therefore, the circularly polarized components of the fractional-order vortex field, Eq. (56), do not contain any phase singularities.

3. *Nonadiabatic following and the hidden phase*

In the continuous uniform isotropic or anisotropic medium only the propagating plane waves participate in the transmitting process. A superposition of the plane waves with preassigned initial phases forms a fractional-order vortex beam. This beam can also be combined with an infinite number of integer-order vortex beams at the initial plane. When propagating, this beam also scatters into integer-order vortex beams with nonmatched Gouy phases.

The situation is absolutely different in a fiber array. Two wave fields—propagating and evanescent (which arise at the cores' boundaries)—influence the shaping of the supermodes of the array. Eigenmodes of each fiber get unified into a propagating supermode, but the mode unification in our case has some important peculiarities. One can speak in a sense about "a mode gluing." The "glue" plays the role of mode coupling between individual fibers, which is implemented through evanescent waves [53]. Such coupling in circular arrays leads to the phenomenon of phase locking, which underlies the forming of supermodes. Due to this effect the phases of individual fiber fields become correlated, which leads to establishing of supermodes. In our case this phase locking is implemented as dictated by the perturbation matrix Eq. (47). If we choose for eigenvector components Eq. (49) then such locking of phases gives contribution to the continuous part of the phase increment on the contour encompassing the array. On the contrary, if one chooses for eigenvector components Eq. (55), which explicitly does not contain any phase part, such contribution is not that evident.

However, this is not the only mechanism of phase increment shaping in arrays. In circular arrays of anisotropic fibers, in addition to the above-mentioned way of accumulating the phase, there is another source of the phase. This source appears when we invoke the effect of *nonadiabatic following*, which is present in such arrays. As was shown in Ref. [48], if the anisotropy is much greater than the interfiber coupling ($k^2\Delta n \gg a$) then when the field evanescently tunnels from one fiber to the adjacent one it loses its initial polarization and acquires a linear polarization directed along the birefringence axis of the neighboring fiber. This process constitutes the essence of nonadiabatic following, at which the field's polarization traces the direction of the anisotropy axes in the array of anisotropic fibers. Due to this phenomenon the local linear polarization in each supermode of the fiber array follows the birefringence axes in the local fibers. Such optical phenomenon has much in common with that of the adiabatic following in a twisted birefringent medium (in particular, in liquid crystals) [54]. In contrast to this classical effect, in our case the matching of the field polarization and the fiber birefringence is realized by jumps as the mode coupling in parallel strongly anisotropic fibers implies.

Quite naturally, the phase at the vertex is not influenced by the director's orientation. However, the global topology of the directors' field comes into effect if one circles around the array's center, e.g., from one vertex to another. Then the inclination angle of the linear polarization in each local fiber accumulates, by jumps, a π increment [see Fig. 11(a)]. Such a polarization evolution is mapped on the Poincaré sphere as a motion along the equator. As a result, each component of the supermode equation (56) with the topological charge $p = 1/2$ acquires the Pancharatnam-Berry phase [55] of $\phi_{\mathrm{PB}} = \pi$ value. This phase increment should be identified with the "hidden phase," the notion of which was first introduced in condensed-matter physics [9].

The prediction of vortices with half of a quantum unit of circulation in superfluid ^{3}He [6] had for a long time been considered as a mathematical misunderstanding. Indeed, a standard superfluid such as uniform ordinary superconductors can also be described in terms of a complex field wave function $\Psi = |\Psi|\, e^{i\Phi}$, where $|\Psi|$ is an amplitude and Φ stands for its phase. In a vortex state the phase can be represented as $\Phi = m\varphi$ with m a vortex charge. The requirement of a single-valuedness of the wave function can be met only for integer m. If the index m takes on a fractional value, the wave function Ψ loses its single-valuedness. However, another situation occurs if the system lacks its homogeneity. For example, it takes place on a boundary between two superconductors (the Josephson junction) or in polycrystalline media on grain boundaries. Pursuing this idea Jang *et al.* have manufactured mesoscopic rings of superconductors (Sr_2RuO_4, strontium ruthenium oxide—an unconventional superconductor that has been proposed as the solid-state analog of the A phase of superfluid ^{3}He) and measured their magnetic moment [7]. As a result, they observed half-flux states with increasing in-plane magnetic field. The following question arose: How it is possible that the Ψ function appears to be not single valued? This paradox was resolved by assuming that there is a hidden phase of π value that is not related to the spin current [9,10]. Our example proves that in optics this hidden phase also exists and has a topological nature.

In spite of such correspondence, in our case this hidden phase is explicitly present in the expressions $\exp(-2i\varphi_p j)\,\sin(\varphi_{2m+1} j)$ and $\exp(2i\varphi_p j)\,\sin(\varphi_{2m+1} j)$ for amplitudes in circular components of the $\tilde{\mathbf{X}}_v$ supermode in a global Cartesian system [see Eqs. (49)–(51)]. Indeed, the multipliers $\exp(\pm 2i\varphi_p j)$ comprise only the information of the array type (through the index p) and not of the specific supermode (whose number is indicated by the index m). The explicit phase increment of the $\mp 2\pi p$ value [that appears only in the global coordinate system (51)] is exactly the Pancharatnam-Berry phase, which has been "hidden" in Ref. [56]. In our case it is the "hydrodynamic" part of the total phase increment that turns out to be hidden. At $p = 1/2$ and $m = 0$ the overall phase increment of 2π, which should take place for a physically meaningful field, is composed of a continuous Pancharatnam-Berry phase increment of π value (which we attribute to a half-vortex charge) and of a phase π jump at the cut of the wave front. The "missing phase" π in our case is nothing else than the π jump that originates due to changing of the sign of the $\sin(\varphi_1 j)$ multiplier while j changes from 0 to $N-1$.

4. *Transmission of fractional and integer-order vortices*

In the above sections we focused our attention mainly on a representation of fractional-order vortices through integer-

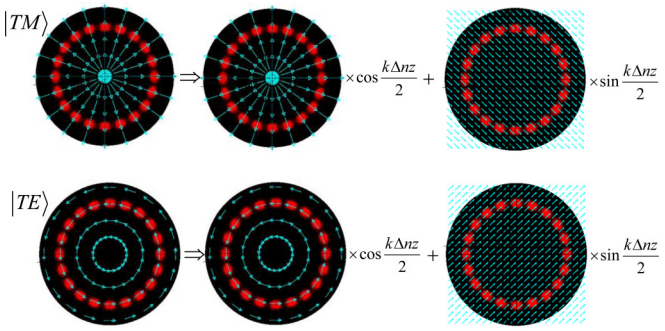

FIG. 15. Diagram of the conversion of |TM⟩ (the upper line) and |TE⟩ (the lower line) states in the fiber array $N = 20$.

order ones. In this subsection we consider an inverse transformation, namely, the representation of the integer-order vortices in terms of half-integer-order ones to standard optical fiber. Let us write the field at the initial z plane as a superposition of supermodes with half-integer-order indices [47]. If we denote the projections of the electric field onto X' and Y' local axes (see Fig. 10) at the jth vertex at $z = 0$ as I_j and L_j, respectively, then the amplitudes $A_\alpha^\pm$ in the right-hand circularly polarized (RCP) and left-hand circularly polarized (LCP) components at the αth fiber at arbitrary length z are written as

$$A_\alpha^\pm = \sum_{v,j} K_v^{j*} K_v^\alpha (I_j e^{i\phi} \mp i L_j e^{-i\phi}) \exp\left(i \frac{P_v}{\tilde{\beta}} z \mp i \gamma_\alpha^p\right), \tag{59}$$

where $\phi = \frac{k\Delta n}{2} z$.

For example, for the input RCP beam at the initial plane $z = 0$ with the amplitude $\sin(n\varphi_j)\exp(-2ij\varphi_q)$ at the jth vertex (n is odd; q is half integer) we obtain the amplitudes at the αth vertex in the form

$$A_\alpha^\pm \sim \sin\left(\alpha\varphi_n - \frac{a}{\tilde{\beta}} z \cos\varphi_{2p} \sin\varphi_{2p-2q} \sin\varphi_n\right) \times \begin{cases} \cos\phi \exp(-i\alpha\varphi_{2q}) \\ i \sin\phi \exp(-i\alpha\varphi_{4q-2q}) \end{cases}. \tag{60}$$

Let us consider the two typical cases.

Case 1. The field of the TM beam is shaped at the $z = 0$ plane of the array with $p = 1/2$. Then the evolution of the |TM⟩ state can be obtained using Eq. (59) as

$$|\mathrm{TM}\rangle = \begin{pmatrix} E_+ \\ E_- \end{pmatrix} \sim \begin{cases} [\cos(\varphi_\alpha + \Phi) - i \sin(\varphi_\alpha - \Phi)] e^{-i\varphi_\alpha} \\ [\cos(\varphi_\alpha - \Phi) + i \sin(\varphi_\alpha + \Phi)] e^{i\varphi_\alpha} \end{cases} = \begin{pmatrix} e^{-2i\varphi_\alpha} \\ e^{2i\varphi_\alpha} \end{pmatrix} \cos\left(\frac{k\Delta n z}{2}\right) + i \begin{pmatrix} 1 \\ 1 \end{pmatrix} \sin\left(\frac{k\Delta n z}{2}\right). \tag{61}$$

The upper line of the diagram in Fig. 15 illustrates transformations of the TM mode. When propagating, the |TM⟩ state is transformed into the |TM⟩ mode itself [the first term in Eq. (61)] and a linearly polarized nonvortex beam with the polarization direction along the ray $\psi = 3\pi/4$ (the second term). At the beating lengths $\Lambda_{\mathrm{TM}} = \frac{2\pi}{k\Delta n}$ and $\Lambda_{lin} = \frac{\pi}{k\Delta n}$ the TM mode and nonvortex beam are alternately recovered.

Similar to that we can find the transformation of the discrete TE field as

$$|\mathrm{TE}\rangle \sim -i \begin{pmatrix} e^{-2i\varphi_a} \\ -e^{2i\varphi_a} \end{pmatrix} \cos\left(\frac{k\Delta n z}{2}\right) - \begin{pmatrix} 1 \\ -1 \end{pmatrix} \sin\left(\frac{k\Delta n z}{2}\right). \tag{62}$$

The |TE⟩ mode is transformed into the |TE⟩ mode itself and a linearly polarized nonvortex beam with the polarization direction along the ray $\psi = \pi/4$ (see the lower line in Fig. 15).

However, the obtained results also show that the nonvortex beam with linear polarization along the ray $\psi = 3\pi/4$ changes into the |TM⟩ mode at the distance $\Lambda = \frac{2\pi}{k\Delta n}$. A simple rotation of the polarizer through an angle $\pi/2$ at the array input turns the |TM⟩ mode into the |TE⟩ one.

Case 2. The RCP vortex beam with the topological charge $l = -1$ is shaped at the $z = 0$ plane. By superposing Eqs. (61) and (62) we obtain the evolution of the discrete integer-order vortex beam as

$$\begin{aligned} |\mathrm{TM}\rangle + i|\mathrm{TE}\rangle = \begin{pmatrix} e^{-i2\varphi_\alpha} \\ 0 \end{pmatrix} &\to \frac{1}{2} \begin{pmatrix} \cos\phi e^{-i2\varphi_\alpha} + i \sin\phi \\ \cos\phi e^{i2\varphi_\alpha} + i \sin\phi \end{pmatrix} \\ &+ \frac{1}{2} \begin{pmatrix} \cos\phi e^{-i2\varphi_\alpha} - i \sin\phi \\ -\cos\phi e^{i2\varphi_\alpha} + i \sin\phi \end{pmatrix} \\ &= \begin{pmatrix} e^{-i2\varphi_\alpha} \\ 0 \end{pmatrix} \cos\frac{k\Delta n z}{2} + i \begin{pmatrix} 0 \\ 1 \end{pmatrix} \sin\frac{k\Delta n z}{2}. \end{aligned} \tag{63}$$

We can also find the evolution of the LCP integer-order vortex,

$$\begin{aligned} |\mathrm{TM}\rangle - i|\mathrm{TE}\rangle = \begin{pmatrix} 0 \\ e^{i2\varphi_\alpha} \end{pmatrix} &\to \begin{pmatrix} 0 \\ e^{i2\varphi_\alpha} \end{pmatrix} \cos\frac{k\Delta n z}{2} \\ &+ i \begin{pmatrix} 1 \\ 0 \end{pmatrix} \sin\frac{k\Delta n z}{2}. \end{aligned} \tag{64}$$

The discrete RCP integer-order vortex $\left(\begin{smallmatrix} e^{-i2\varphi_\alpha} \\ 0 \end{smallmatrix}\right)$ goes into itself and a LCP nonvortex beam while the LCP integer-order vortex $\left(\begin{smallmatrix} 0 \\ e^{i2\varphi_\alpha} \end{smallmatrix}\right)$ goes into itself and a RCP nonvortex beam. In essence, the fiber array with $p = 1/2$ transforms the RCP beam with topological charge $l < 0$ and the LCP beam with $p > 0$ into itself and the vortex beam with the opposite circular polarization and $l - 1$ charge.

V. CONCLUSION

In this paper we have considered a variety of vector fractional-order vortex beams that could be transmitted through free space or a uniform isotropic medium without structural decay. Among them the Gamma-Gaussian beams bearing half-integer-order vortices occupy a special place because they are met not only in optical experiments but also are the objects of unchanging attention in the physics of superconductors. However, we revealed that all types of such vortex beams are unstable under propagation in unbounded uniform isotropic and birefringent media, in particular, in biaxial crystals under the condition of conical diffraction. A typical scenario of the beam propagation in the biaxial crystals evolves in such a way that the topological charges of the fractional-order vortices in the circularly polarized

components of vector beams differ from each other by one unit. The difference between the propagation constants of the components is independent of the topological charge value. The beam structure is broken down due to a mismatching of the Gouy phases in partial singular beams in the vortex spectrum of the fractional-order vortex beam.

On the other hand, we showed that singular beams with the stable centered integer-order vortices but a complex framing can be formed by four fractional-order vortices. Such constructions remain stable under propagation for different values of the topological charges.

An absolutely different situation occurs in the birefringent fiber array, where fractional-order vortices are supermodes. The shaping of the array supermode is mediated by evanescent coupling between the modes of the neighboring fibers that leads to the phase-locking process over the array.

Special attention is paid to the problem of the hidden phase in the fiber array first introduced in the physics of superconductivity to explain the origin of fractional vortices in superconductors. We showed that the integer-charge phase increment in a fractional-order supermode consists of two half-integer-charge phase contributions. The explicit phase contribution is connected with the Pancharatnam-Berry phase that arises due to the phenomenon of nonadiabatic following. The implicit half-integer-charge phase contribution (or the "hidden phase") comes due to the sign alteration of the amplitude factors in the field components that corresponds to the wave-front cuts. We have also made the comparison of the hidden and hydrodynamic phases in superfluidic fractional-charge vortices with analogous phases in fractional-order supermodes. We have established that in the optical case the hidden phase corresponds to the hydrodynamic phase in superfluids, whereas the hidden superfluidic phase is the analog of the optical Pancharatnam-Berry phase in supermodes.

We showed also that the vector field bearing integer-order vortices cannot propagate through the fiber array without the periodical decay and recovery of its inner structure. In this sense we can speak of optical quarks introduced in the Standard Model of particle physics. The optical quarks can exist only inside the medium with an appropriate structural symmetry. Outside the medium, the optical quarks are transformed into a set of integer-order vortices.

ACKNOWLEDGMENTS

A.V. thanks V. Belyi and N. Khilo for the useful discussion on the conical diffraction process in biaxial crystals and E. Abramochkin for the discussion on the nonfactorized paraxial beams. C.A. acknowledges support of the Russian Foundation for Basic Research (RFBR) (Grant No. 16-07-00759).

[1] M. S. Soskin and M. V. Vasnetsov, Prog. Opt. **42**, 219 (2001).
[2] I. Basistiy, M. Soskin, and M. Vasnetsov, Opt. Commun. **119**, 604 (1995).
[3] I. Basistiy, V. Pas'ko, V. Slyusar, M. Soskin, and M. Vasnetsov, J. Opt. A: Pure Appl. Opt. **6**, S166 (2004).
[4] M. V. Berry, R. G. Chambers, M. D. Large, C. Upstill, and J. C. Walmsley, Eur. J. Phys. **1**, 154 (1980).
[5] M. V. Berry, J. Opt. A: Pure Appl. Opt. **6**, 259 (2004).
[6] G. E. Volovik and V. P. Mineev, Pis'ma Zh. Eksp. Teor. Fiz. **24**, 605 (1976).
[7] J. Jang, D. G. Ferguson, V. Vakaryuk, R. Budakian, S. B. Chung, P. M. Goldbart, and Y. Maeno, Science **331**, 186 (2011).
[8] S. W. Seo, S. Kang, W. J. Kwon, and Yong-il Shin, Phys. Rev. Lett. **116**, 079901 (2016).
[9] J. A. Sauls, Physics **9**, 148 (2016).
[10] A. Hansen, J. T. Schuliz, and N. P. Bigelow, Optica **3**, 355 (2016).
[11] S. Tao, W. Lee, and X. Yuan, Appl. Opt. **43**, 122 (2004).
[12] J. Leach, E. Yao, and M. J. Padgett, New J. Phys. **6**, 71 (2004).
[13] H. Garcia and J. Gutierrez-Vega, J. Opt. Soc. Am. A **26**, 794 (2009).
[14] J. C. Gutiérrez-Vega and C. López-Mariscal, J. Opt. Soc. Am. A **10**, 015009 (2008).
[15] F. G. Mitri, Opt. Lett. **36**, 606 (2011).
[16] Y. Fang, Q. Lu, X. Wang, W. Zhang, and L. Chen, Phys. Rev. A **95**, 023821 (2017).
[17] T. A. Fadeyeva, C. Alexeyev, A. Rubass, and A. Volyar, Opt. Lett. **37**, 1397 (2012).
[18] T. A. Fadeyeva, A. F. Rubass, R. V. Aleksandrov, and A. V. Volyar, J. Opt. Soc. Am. B **31**, 798 (2014).
[19] V. V. Kotlyar, A. A. Kovalev, and V. A. Soifer, Comput. Opt. **38**, 4 (2014)
[20] G. Maleshkov, D. N. Neshev, and A. Dreischuh, Phys. Rev. A **80**, 053828 (2009).
[21] C. Alexeyev, A. Kovalyova, A. Rubass, A. Volyar, and M. Yavorsky, Opt. Lett. **42**, 783 (2017).
[22] A. P. Kiselev, Opt. Spectrosc. **96**, 479 (2004).
[23] F. Cardano, E. Karimi, S. Slussarenko, L. Marrucci, Corrado de Lisio, and E. Santamato, Appl. Opt. **51**, C1 (2012).
[24] D. Song, C. Lou, L. Tang, Z. Ye, J. Xu, and Z. Chen, Int. J. Opt. **2012**, 273857 (2012).
[25] A. Yu. Okulov, J. Mod. Opt. **55**, 241 (2008).
[26] T. Fadeyeva, A. Rubass, I. Valkov, and A. Volyar, J. Opt. **15**, 044020 (2013).
[27] A. P. Prudnikov, Yu. A. Brychkov, and O. I. Marichev, *Integrals and Series* (Nauka, Moskva, 1981), Vol. 1, p. 799.
[28] M. V. Berry and M. R. Jeffrey, Prog. Opt. **50**, 13 (2007).
[29] M. V. Berry, M. R. Jeffrey, and J. G. Lunney, Proc. R. Soc. A **462**, 1629 (2006).
[30] I. Skab, Yu. Vasylkiv, V. Savaryn, and R. Vlokh, J. Opt. Soc. Am. A **28**, 633 (2011).
[31] I. Skab, Yu. Vasylkiv, V. Savaryn, and R. Vlokh, Ukr. J. Phys. Opt. **11**, 193 (2010).
[32] T. A. Fadeyeva, C. N. Alexeyev, P. M. Anischenko, and A. V. Volyar, Appl. Opt. **51**, C1 (2012).
[33] Yu. A. Egorov, T. A. Fadeyeva, and A. V. Volyar, J. Opt. A: Pure Appl. Opt. **6**, S217 (2004).
[34] N. S. Kazak, N. A. Khio, and A. A. Ryzhevich, Quantum Electron. **29**, 1020 (1999).
[35] V. Belyi, T. King, N. Kazak, N. Khio, E. Katranji, and A. Ryzhecich, Proc. SPIE **4403**, 229 (2001).
[36] V. N. Belyi, N. A. Khilo, S. N. Kurilkina, and N. S. Kazak, J. Opt. **15**, 044018 (2013).
[37] T. King, W. Hogervorst, N. Kazak, N. Khilo, and A. Ryzhevich, Opt. Commun. **187**, 407 (2001).

[38] N. A. Khilo, Opt. Commun. **286**, 1 (2013).
[39] L. Marrucci, E. Karimi, S. Slussarenko, B. Piccirillo, E. Santamato, E. Nagali, and F. Sciarrino, J. Opt. **13**, 064001 (2011).
[40] S. Slussarenko, A. Murauski, T. Du, V. Chigrinov. L. Marrucci, and E. Santamato, Opt. Express **19**, 4085 (2011).
[41] F. Cardano, E. Karimi, L. Marrucci, Corrado de Lisio, and E. Santamato, Opt. Express **21**, 8815 (2013).
[42] A. V. Volyar, Ukr. J. Phys. Opt. **14**, 31 (2013).
[43] T. Ritari, H. Ludvigsen, M. Wegmuller, M. Legré, N. Gisin, J. R. Folkenberg, and M. D. Nielsen, Opt. Express **12**, 5943 (2004).
[44] A. Bezryadina, D. Neshev, A. Desyatnikov, J. Young, Z. Chen, and Yu. Kivshar, Opt. Express **14**, 8317 (2006).
[45] Y. S. Lee, C. G. Lee, Y. Jung, M.-k. Oh, and S. Kim, J. Opt. Soc. Korea **20**, 567 (2016).
[46] C. N. Alexeyev, A. V. Volyar, and M. A. Yavorsky, Phys. Rev. A **80**, 063821 (2009).
[47] C. N. Alexeyev, A. O. Pogrebnaya, G. Milione, and M. A. Yavorsky, J. Opt. **18**, 025602 (2016).
[48] C. N. Alexeyev, J. Opt. **15**, 4 (2013).
[49] S. S. M. Wong, *Introductory Nuclear Physics*, 2nd ed. (Wiley Interscience Publication, New York, 1998), p. 460.
[50] A. Yariv and P. Yeh, *Optical Waves in Crystals* (John Wiley & Sons, New York, 1984), p. 589.
[51] A. V. Volyar, Yu. A. Egorov, A. F. Rubass, and T. A. Fadeeva, Tech. Phys. Lett. **30**, 701 (2004).
[52] M. R. Dennis, Opt. Commun. **213**, 201 (2002).
[53] F. de Fornel, *Evanescent Waves* (Springer, Heidelberg, 2001), p. 265.
[54] M. V. Berry, J. Opt. A **11**, 094001 (2009).
[55] J. C. Gutiérrez-Vega, Opt. Lett. **36**, 1143 (2011).
[56] S. N. Alperin, R. D. Niederriter, J. T. Gopnath, and M. E. Siements, Opt. Lett. **41**, 5019 (2016).